厚生労働科学研究費補助金　(肝炎等克服緊急対策研究事業)
分担研究報告書

ウイルス肝炎による肝がんの再発防止メカニズムの解明に関する研究

進行肝癌に対する治療法の検討

研究分担者：金井文彦　千葉大学医学附属病院　講師

研究要旨：肝癌の予後改善には，再発機構を明らかにして，防止策を構築することが重要である．一方，進行肝細胞癌の生命予後を改善することが初めて示されたソラフェニブもようやく本邦でも承認された．進行癌に対する効果のみならず，根治術後や TACE 後の再発防止の補助療法としての有効性も期待されている．本研究では，本邦での承認後使用成績をまとめ，海外の臨床試験成績と比較検討した．

A. 研究目的

ソラフェニブは進行肝細胞癌に対し、有意に全生存期間 (OS) の延長を示した初の分子標的薬である。2009 年 5 月以降本邦でも使用可能となったが、ソラフェニブ特有の有害事象も報告されている。進行肝細胞癌に対するソラフェニブの実地臨床における安全性と有効性について検討をおこなった。

B. 研究方法

ソラフェニブを投与された 50 症例について、有害事象を CTCAE v3.0、抗腫瘍効果を RECIST に準じてレトロスペクティブに解析を行った。

C. 研究結果

年齢中央値 67.5 歳(48-82 歳)、男/女 43/7、BCLC B/C 32/18、Child-Pugh 分類 A/B 41/9 (5/6/7/8　21/20/6/3)、肝癌治療歴 有/無 48/2 であった。抗腫瘍効果 (n=26) は CR/PR/SD/PD 0/0/18/8 と CR および PR は認めなかった。手足皮膚反応 (以下 HFSR) は 43 例で認め、23 例は HFSR を理由に減量・休薬を必要とした。減量・休薬を必要とした 23 例中 21 例は 4 週間以内に減量を行い、うち 16 例は以後 HFSR での減量は必要としなかった。4 例は HFSR を理由に治療中止となった。4 週間以内に Grade 3 以上のトランスアミラーゼ上昇を 9 例に認め、いずれも減量・休薬を必要とした。これら 9 症例の開始前の Child-Pugh 分類は A/B/C 7/2/0 であったが、トランスアミラーゼ上昇後 6 症例で Child-Pugh score の 2 点以上の悪化を認め、うち 3 症例に肝性脳症を、1 症例に著明な腹水の増加を認めた。これら 6 症例中 5 症例例は治療中止となった。

D. 考察

HFSR は高率で出現するものの、減量・休薬によりコントロール可能な症例が多い。海外の大規模臨床試験とは異なり、治療開始早期に肝機能障害を認める症例が散見される。治療開始前の肝機能が良好な症例でも急激な肝機能悪化を認める場合もあり、患者背景と肝機能障害の関連を検討する必要がある

E. 結論

ソラフェニブの海外の臨床試結果が，我国の臨床現場にあてはなるかどうか，有効性・安全性を検討した．再発防止効果については今後の検討課題である．

F. 健康危険情報

ソラフェニブは Child-Pugh B の肝機能障害

を持つ患者に対する安全性は確立していない.

G. 論文発表

1. Tateishi R, Shiina S, Ohki T, Sato T, Masuzaki R, Imamura J, Goto E, Goto T, Yoshida H, Obi S, Sato S, Kanai F, Yoshida H, Omata M. Treatment strategy for hepatocellular carcinoma: expanding the indications for radiofrequency ablation. J Gastroenterol. 2009;44:S142-S146.
2. Ohki T, Tateishi R, Shiina S, Goto E, Sato T, Nakagawa H, Masuzaki R, Goto T, Hamamura K, Kanai F, Yoshida H, Kawabe T, Omata M. Visceral Fat Accumulation Is an Independent Risk Factor of Hepatocellular Carcinoma Recurrence after Curative Treatment in NASH-suspected Patients. Gut. 2009;58:839-844.
3. Masuzaki R, Tateishi R, Yoshida H, Goto E, Sato T, Ohki T, Imamura J, Goto T, Kanai F, Kato N, Ikeda H, Shiina S, Kawabe T, Omata M. Prospective Risk Assessment for Hepatocellular Carcinoma Development in Chronic Hepatitis C Patients by Transient Elastography. Hepatology. 2009;49:1954-1961.
4. Nakamoto S, Kanda T, Yonemitsu Y, Arai M, Fujiwara K, Fukai K, Kanai F, Imazeki F, Yokosuka O. Quantification of hepatitis C amino acid substitutions 70 and 91 in core coding region by real-time amplification refractory mutation system reverse transcription-polymerase chain reaction. Scand J Gastroenterol. 2009;44:872-827.
5. Sato T, Tateishi R, Yoshida H, Ohki T, Masuzaki R, Imamura J, Goto T, Kanai F, Obi S, Kato N, Shiina S, Kawabe T, Omata M. Ultrasound surveillance for early detection of hepatocellular carcinoma among patients with chronic hepatitis C. Hepatology International. 2009;3:544-550.
6. Ohki T, Tateishi R, Goto E, Sato T, Masuzaki R, Imamura J, Goto T, Kanai F, Kato N, Shiina S, Yoshida H, Kawabe T, Omata M. Influence of anti-HBc seropositivity on the risk of hepatocellular carcinoma in HCV-infected patients after adjusting for confounding factors. J Viral Hepat. 2010;17:91-97.
7. Asaoka Y, Kanai F, Ichimura T, Tateishi K, Tanaka Y, Ohta M, Seto M, Tada M, Ijichi H, Ikenoue T, Kawabe T, Isobe T, Yaffe MB, Omata M. Identification of a suppressive mechanism for hedgehog signaling through a novel interaction of Gli with 14-3-3. J Biol Chem 2010;285:4185-4194.

学会発表

1. 金井文彦，小俣政男：肝細胞癌に対する血管新生阻害剤TSU-68の治療効果予測因子. 第45回日本肝臓学会総会ワークショップ「肝癌発生・進展の分子機構と臨床への還元」，2009，神戸.
2. Nakamoto S, Imazeki F, Fukai K, Fujiwara K, Arai M, Kanda T, Kanai F, Yokosuka O.: Association of hepatitis C virus core mutation with hepatocarcinogenesis. The 13th International Symposium on Viral Hepatitis and Liver disease, 2009, Washington.
3. Kanda T, Imazeki F, Nakamoto S, Okitsu K, Arai M, Fujiwara K, Fukai K, Kanai F, Yokosuka O. Clinical isolates-derived HAV IRES-mediated translations are inhibited by amantadine in human hepatoma cells. The 13th International Symposium on Viral Hepatitis and Liver disease, 2009, Washington.
4. Okabe S, Yoshikawa M, Suzuki Y, Kitayama C, Ito R, Sakurada T, Sato N, Shinozaki Y, Kanai F, Sunaga M, Ueda S, Yokosuka O. Relationship between vascular endothelial growth factor and its receptor gene expression

in hepatocellular carcinoma and its surrounding liver parenchyma. The 19th Conference of the Asian Pacific Association for the Study of the Liver (APASL), 2009, Hong Kong.

5. Shinozaki Y, Yoshikawa M, Okabe S, Kanai F, Sunaga M, Yokosuka O. Efficacy of transarterial chemo-lipiodolization using cisplatin powder delivered via an injection port for advanced hepatocellular carcinoma. The 19th Conference of the Asian Pacific Association for the Study of the Liver (APASL), 2009, Hong Kong.
6. Enooku K, Tateishi R, Kanai F, Yoshida H, Sato T, Ohki T, Masuzaki R, Imamura J, Yamashiki N, Goto T, Shiina S, Kawabe T, Omata M.: Evaluation of the effects of antiangiogenic drug by changes in tumor marker levels. Digestive Disease Week 2009, 2009, Chicago.
7. Shinozaki Y, Yoshikawa M, Okabe S, Sunaga M, Kanai F, Yokosuka O. Hepatic arterial infusion chemotherapy by using injection port for advanced hepatocellular carcinoma resistant to TACE. The 5th APASL Single Topic Conference, 2009, Istanbul.

H. 知的財産権の出願・登録状況

(予定を含む)

特許取得：なし

実用新案登録：なし

その他：なし

研究成果の刊行に関する一覧表

発表者氏名	論文タイトル名	発表誌名	巻名	ページ	出版年
Masuzaki R, Yoshida H, Tateishi R, Omata M.	Staging systems: is there a surgical staging and a medical one? : Hepatologist's perspective.	J Hepatobiliary Pancreat Surg		In press	2010
Asaoka Y, Kanai F, Ichimura T, Tateishi K, Tanaka Y, Ohta M, Seto M, Tada M, Ijichi H, Ikenoue T, Kawabe T, Isobe T, Yaffe MB, Omata M.	Identification of a suppressive mechanism for hedgehog signaling through a novel interaction of Gli with 14-3-3.	J Biol Chem	285	4185-4194	2010
Masuzaki R, Yamashiki N, Sugawara Y, Yoshida H, Tateishi R, Tamura S, Kaneko J, Hasegawa K, Kokudo N, Makuuchi M, Omata M.	Assessment of liver stiffness in patients after living donor liver transplantation by transient elastography.	Scand J G astroenterol	44	1115-1120	2009
Masuzaki R, Tateishi R, Yoshida H, Goto E, Sato T, Ohki T, Imamura J, Goto T, Kanai F, Kato N, Ikeda H, Shiina S, Kawabe T, Omata M.	Prospective risk assessment for hepatocellular carcinoma development in chronic hepatitis C patients by transient elastography.	Hepatology	49	1954-1961	2009
Nakamoto S, Kanda T, Yonemitsu Y, Arai M, Fujiwara K, Fukai K, Kanai F, Imazeki F, Yokosuka O.	Quantification of hepatitis C amino acid substitutions 70 and 91 in core coding region by real-time amplification refractory mutation system reverse transcription-polymerase chain reaction.	Scand J Gastroenterol	44	872-877	2009
Nomura H, Miyagi Y, Tanimoto H, Ishibashi H.	Impact of early viral kinetics on pegylated interferon alpha 2b plus ribavirin therapy in Japanese patients with genotype 2 chronic hepatitis C.	J Viral Hepatitis	16	346-351	2009
Nomura H, Miyagi Y, Tanimoto H, Higashi M, Ishibashi H.	Effective prediction of outcome of combination therapy with pegylated interferon alpha 2b plus ribavirin in Japanese patients with genotype-1 chronic hepatitis C using early viral kinetics and new indices.	J Gastroenterol	44	338-345	2009
Ohki T, Tateishi R, Shiina S, Goto E, Sato T, Nakagawa H, Masuzaki R, Goto T, Hamamura K, Kanai F, Yoshida H, Kawabe T, Omata M.	Visceral fat accumulation is an independent risk factor for hepatocellular carcinoma recurrence after curative treatment in patients with suspected NASH.	Gut	58	839-844	2009
Ohki T, Tateishi R, Goto E, Sato T, Masuzaki R, Imamura J, Goto T, Kanai F, Kato N, Shiina S, Yoshida H, Kawabe T, Omata M.	Influence of anti-HBc seropositivity on the risk of hepatocellular carcinoma in HCV-infected patients after adjusting for confounding factors.	J Viral Hepat	17	91-97	2009
Sato T, Tateishi R, Yoshida H, Ohki T, Masuzaki R, Imamura J, Goto T, Kanai F, Obi S, Kato N, Shiina S, Kawabe T, Omata M.	Ultrasound surveillance for early detection of hepatocellular carcinoma among patients with chronic hepatitis C.	Hepatol Int	3	544-550	2009

Shiina S.	Image-guided percutaneous ablation therapies for hepatocellular carcinoma.	J Gastroenterol	44	S122-S131	2009
Tateishi R, Shiina S, Ohki T, Sato T, Masuzaki R, Imamura J, Goto E, Goto T, Yoshida H, Obi S, Sato S, Kanai F, Yoshida H, Omata M.	Treatment strategy for hepatocellular carcinoma: expanding the indications for radiofrequency ablation.	J Gastroenterol	44	S142-S146	2009
Yamashiki N, Sugawara Y, Tamura S, Kaneko J, Matsui Y, Togashi J, Kokudo N, Omata M, Makuuchi M.	Doube-dose-phase use of second generation heptatitis B virus vaccine in patients after living donor liver transplantation: not an effective measure in transplant recipient.	Hepatol Res	39	7-13	2009

THE JOURNAL OF BIOLOGICAL CHEMISTRY VOL. 285, NO. 6, pp. 4185–4194, February 5, 2010

Identification of a Suppressive Mechanism for Hedgehog Signaling through a Novel Interaction of Gli with 14-3-3*

Received for publication, June 28, 2009, and in revised form, November 29, 2009 Published, JBC Papers in Press, December 7, 2009, DOI 10.1074/jbc.M109.038232

Yoshinari Asaoka[‡1], Fumihiko Kanai[§], Tohru Ichimura[¶], Keisuke Tateishi[‡], Yasuo Tanaka[‡], Miki Ohta[‡], Motoko Seto[‡], Motohisa Tada[§], Hideaki Ijichi[‡], Tsuneo Ikenoue[‡], Takao Kawabe[‡‖], Toshiaki Isobe[**], Michael B. Yaffe[‡‡], and Masao Omata[‡]

From the Departments of [‡]Gastroenterology and [‖]Endoscopy and Endoscopic Surgery, Graduate School of Medicine, The University of Tokyo, Tokyo 113-8655, Japan, the [§]Departments of Medicine and Clinical Oncology, Graduate School of Medicine, Chiba University, Chiba 260-8677, Japan, the [¶]Department of Applied Chemistry, National Defense Academy, Kanagawa 239-8686, Japan, the [**]Department of Chemistry, Graduate School of Science, Tokyo Metropolitan University, Tokyo 192-0397, Japan, and the [‡‡]Center for Cancer Research and Departments of Biology and Biological Engineering, Massachusetts Institute of Technology, Cambridge, Massachusetts 02139

Gli transcription factors are central effectors of Hedgehog signaling in development and tumorigenesis. Using a tandem affinity purification (TAP) strategy and mass spectrometry, we have found that Gli1 interacts with 14-3-3ϵ, and that Gli2 and Gli3 also bind to 14-3-3ϵ through homologous sites. This interaction depends on their phosphorylation, and cAMP-dependent protein kinase (PKA), a known negative regulator of Hedgehog signaling serves as a responsible kinase. A Gli2 mutant engineered to eliminate this interaction exhibited increased transcriptional activity (2 ~ 3×). Transcriptional repression by 14-3-3 binding was also observed with Gli3, when its N-terminal repressor domain was deleted. The phosphorylation sites responsible for the binding to 14-3-3 are distinct from those required for proteolysis, the known mechanism for PKA-induced repression of Hh signaling. Our data propose a novel mechanism in which PKA down-regulates Hedgehog signaling by promoting the interaction between Gli and 14-3-3 as well as proteolysis. Given the certain neuronal or malignant disorders in human caused by the abnormality of 17p13 encompassing 14-3-3ϵ overlap with increased Hh signaling, the Gli-14-3-3 interaction may have pathological significance for those human diseases.

The signaling proteins of the Hedgehog (Hh)[2] family play central roles in many developmental processes in organisms from flies to humans, particularly processes involving patterning of the neural tube, notochord, and prechordal mesoderm (1, 2). Hedgehog protein, the ligand that initiates Hh signal transduction pathway, is a developmental morphogen that elicits a graded cellular response depending on the distance between the recipient cell and the ligand-secreting cell. This gradient-dependent signaling is thought to be important in the determination of cell fate. Deregulation of Hh signaling results in a variety of congenital malformations and cancers (3–5). Given the importance of the Hh signaling pathway, there has been considerable interest in understanding the mechanism by which a target cell interprets Hh signaling to yield an appropriate response.

In *Drosophila*, activation and repression of Hh target genes is mediated by a single Gli zinc finger transcription factor known as Cubitus interruptus (Ci). In the absence of Hh signaling, Ci is phosphorylated by cAMP-dependent protein kinase (PKA) (6), glycogen synthase kinase 3β (GSK3β), and casein kinase I (CKI). After proteolytic processing into an N-terminal repressor form, Ci translocates to the nucleus, where it silences expression of its target genes. Hh signaling triggers a series of events that prevents this phosphorylation and proteolysis of Ci, to block formation of the repressor form, and allow the full-length, activating form of Ci to enter the nucleus and promote induction of specific target genes (1, 7).

In vertebrates, three Hedgehog proteins (sonic, Indian, and desert), and three Gli proteins, Gli1, Gli2, and Gli3, are involved in transcriptional control of Hh target genes (2, 8). Each Gli protein has a unique role: Gli3 functions chiefly as a transcriptional repressor, Gli2 is chiefly a transcriptional activator, and Gli1 functions only as a transcriptional activator (1). Like Ci, Gli3 is phosphorylated and processed in the absence of Hh; it responds to Hh by relocalizing to the nucleus without cleavage (9). Though Gli1 knockout mice develop normally, Gli2 and Gli3 knockouts have serious developmental abnormalities (4), suggesting that Gli2 and Gli3 signaling is likely to be intensely regulated in response to Hh ligands. To better understand the molecular mechanisms underlying Gli activation and regulation, we used a tandem affinity purification (TAP) strategy involving a novel mammalian TAP tag, called MEF (10, 11), in conjunction with mass spectrometry, to isolate and characterize human protein complexes containing Gli.

EXPERIMENTAL PROCEDURES

Cell Cultures and Transient Transfection—The human embryonic kidney cell line 293T, the human hepatoma cell line PLC/PRF/5, the human cervical carcinoma cell line HeLa, and the mouse fibroblast cell line NIH3T3 (Riken Cell Bank, Tsukuba Science City, Japan) were maintained in Dulbecco's

* This work was supported, in whole or in part, by National Institutes of Health Grant GM60594 (to M. B. Y.).

[1] To whom correspondence should be addressed: 7-3-1 Hongo, Bunkyo-ku, Tokyo 113-8655, Japan. Fax: 81-3-3814-0021; E-mail: yasa-tky@umin.ac.jp.

[2] The abbreviations used are: Hh, Hedgehog; Ci, Cubitus interruptus; SUFU, Suppressor of Fused; PKA, cAMP-dependent kinase; PKA-CA, PKA constitutively active subunit; FSK, forskolin; SAG, Smo agonist; pSer, phosphoserine; pThr, phosphothreonine; wt, wild type; Ab, antibody; EYFP, enhanced yellow fluorescent protein; TAP, tandem affinity purification; GST, glutathione *S*-transferase; HRP, horseradish peroxidase.

modified Eagle's medium (Sigma) containing 10% heat-inactivated fetal bovine serum (293T, PLC/PRF/5, and HeLa) or bovine serum (NIH3T3). All cells were incubated at 37 °C and 5% CO_2. Cells were seeded on culture plates, and transfections were carried out using Effectene transfection reagent (Qiagen, Hilden, Germany) for PLC/PRF/5 and NIH3T3 cells or FuGENE 6 (Roche Applied Science, Indianapolis, IN) for 293T and Hela cells, as described in the manufacturers' protocol.

Antibodies and Materials—Mouse monoclonal anti-c-Myc Ab (9E10) and its agarose-conjugated form, rabbit polyclonal anti-14-3-3 Ab (K-19), and normal rabbit IgG were obtained from Santa Cruz Biotechnology (Santa Cruz, CA). Mouse monoclonal anti-FLAG M2 Ab and its agarose-conjugated form and mouse monoclonal anti-α-tubulin Ab (DM1A) were purchased from Sigma. Mouse monoclonal anti-Xpress Ab was obtained from Invitrogen (Carlsbad, CA), and mouse monoclonal Ab (4E2) specific for the phospho-(Ser) 14-3-3 binding motif, rabbit monoclonal Ab (100G7E) specific for the phospho-PKA substrate, and rabbit polyclonal anti-Gli1 (nos. 2553 and 2534) and anti-14-3-3ϵ Abs were from Cell Signaling Technology (Beverly, MA). Alexa Fluor 488 goat anti-mouse IgG secondary Ab was obtained from Molecular Probes (Eugene, OR). Horseradish peroxidase (HRP)-conjugated anti-mouse and anti-rabbit Abs were purchased from GE Healthcare (Piscataway, NJ). Forskolin (FSK) and Smo agonist (SAG) were obtained from Sigma and Alexis Biochemicals, respectively.

Plasmids—Human Gli1 and Gli3 cDNAs (from K. W. Kinzler and B. Vogelstein (2, 8)) and mouse Gli2 cDNA (from H. Sasaki (12)) with deletions of their 5′-untranslated sequences were cloned into the vector pcDNA3-MEF, a mammalian expression plasmid for the MEF method described previously (10, 11). PCR-based mutagenesis was used, and genes encoding wt and mutant ΔN-Gli3 were prepared utilizing the unique BamHI site. ΔPKA-Gli2 was generated by a combination of restriction digestion and PCR strategies to delete the region from Ser-781 to Leu-861. All PCR-generated constructs were verified by sequencing. The reporter plasmid GliBS-Luc, the Myc-tagged SUFU expression vector, the vector expressing the constitutively active catalytic subunit of PKA (PKA-CA), and the 14-3-3 inhibitor peptide expression vector EYFP-difopein were kindly provided by H. Sasaki (13), R. Toftgard (14), G.S. McKnight (15), and H. Fu (16), respectively.

MEF Purification and Tandem Mass Spectrometry—MEF purification was carried out as described previously (10, 11). Briefly, 40 10-cm dishes containing ~8×10^7 293T cells in total were transfected with 80 μg of pcDNA3-MEF-GLI1 or pcDNA3-MEF plasmid. After 48 h, the cells were harvested in lysis buffer (50 mM Tris-HCl, pH 7.5, 150 mM NaCl, 10% (w/v) glycerol, 100 mM NaF, 10 mM EGTA, 1 mM Na_3VO_4, 5 μM $ZnCl_2$, 0.05% SDS, 1% (w/v) Nonidet P-40, and a protease inhibitor mixture (Complete Mini; Roche Applied Science)), and centrifuged at 15,000 × *g* for 20 min at 4 °C. The supernatant fraction was removed and incubated with anti-Myc Ab-conjugated agarose beads for 90 min at 4 °C. The beads were then washed five times with wash buffer (20 mM Tris-HCl (pH 7.5), 150 mM NaCl, 10% (w/v) glycerol, 0.05% SDS, 0.1% (w/v) Nonidet P-40) and twice with buffer B (50 mM Tris-HCl (pH 8.0), 150 mM NaCl, 0.05% SDS, 0.1% (w/v) Nonidet P-40). The beads were then mixed with 15 units of tobacco etch virus (TEV) protease (Invitrogen) in buffer B at room temperature for 1 h to release the protein complex from the beads.

The protein complex was incubated with anti-FLAG Ab-conjugated agarose beads for a second immunoprecipitation at room temperature for 1 h. After three washes with buffer A (20 mM Tris-HCl, pH 7.5, 150 mM NaCl), the beads were eluted with FLAG peptide (80 μg/ml) in buffer A. The eluted proteins were concentrated, separated by 10/20% SDS-PAGE, and visualized by silver staining.

Protein bands were excised from the gel and digested with trypsin, and the resultant peptide fragments were analyzed using a direct nano-flow LC-MS/MS system equipped with an electrospray interface reversed-phase column, a nano-flow gradient device, and a high-resolution quadrupole time-of-flight hybrid mass spectrometer (Q-TOF2; Micromass, Manchester, UK). To identify the proteins, all of the MS/MS spectra were searched against the non-redundant protein sequence data base maintained at the National Center for Biotechnology Information using the Mascot program (Matrixscience, London, UK). The MS/MS signal assignments were confirmed manually.

Immunoprecipitation and Immunoblotting—Immunoprecipitation and immunoblotting were performed as previously described (11, 17). After 293T cells were lysed, the cellular proteins were incubated with anti-FLAG agarose-conjugated beads for 1 h at 4 °C. To detect endogenous interaction, cell lysates from PLC/PRF/5 cells were incubated for 1 h at 4 °C with anti-Gli1 or anti-14-3-3ϵ Ab or normal IgG control, followed by an additional 4 h of incubation with protein G. The beads were then washed, and the immunoprecipitated proteins were eluted by boiling in SDS sample buffer. The proteins were separated by SDS-PAGE and electrophoretically transferred to a polyvinylidene difluoride membrane. The membrane was probed with primary Ab (anti-14-3-3, anti-14-3-3ϵ, anti-Gli1, anti-phospho-14-3-3 binding site, anti-phospho-PKA substrate, anti-Xpress, anti-Myc, or anti-FLAG at 1:1,000 dilution, and anti-α-tubulin at 1:5000) and with secondary Ab (HRP-conjugated anti-mouse or anti-rabbit Ab at 1:1000 to 1:5000 dilution). The HRP signal was detected using an enhanced chemiluminescence system (ECL Plus, GE Healthcare).

Expression and Purification of Recombinant Gli1, Gli2, and Gli3 Proteins and in Vitro Kinase Assay—The regions surrounding the 14-3-3 binding sites on Gli1 (aa 617–688), Gli2 (aa 924–1057), and Gli3 (aa 981–1101) were amplified by PCR and inserted in-frame into the BamHI and XhoI (Gli1) or NotI (Gli2 and Gli3) sites of vector pGEX-6P-1 (GE Healthcare). The resulting expression vectors were transformed into *Escherichia coli* BL21(DE3) cells (Stratagene). Expression was induced with 1 mM isopropyl-1-thio-β-D-galactopyranoside at 25 °C for 3 h. The cells were then pelleted and lysed in a buffer consisting of 50 mM Tris-HCl, pH 8.0, 2 mM EDTA, 1 mM dithiothreitol, 1 mg/ml lysozyme, and 1% Triton X-100. The lysates were sonicated and clarified by centrifugation (10,000 × *g* for 10 min at 4 °C). The fusion proteins were purified from the cleared bacterial lysates using glutathione-Sepharose 4B (GE Healthcare).

Purified GST fusion proteins were incubated with 25 ng of recombinant PKA catalytic subunit (Upstate, Lake Placid, NY),

20 μl of Assay Dilution Buffer I (Upstate) containing 10 μg of bovine serum albumin, and Magnesium/ATP Mixture (Upstate) containing 10 μCi of [γ-^{32}P]ATP (GE Healthcare). After 30 min at 30 °C, the reactions were terminated by addition of 13 μl of 4× SDS-PAGE sample buffer, and phosphorylated proteins were visualized by SDS-PAGE and autoradiography.

Knockdown of 14-3-3ε using Lentiviral-based shRNA Vector—pLKO.1-based lentiviral 14-3-3ε shRNA vectors, TRCN0000062233 and 000062236 for PLC/PRF/5 and TRCN0000012385 and 0000012386 for NIH3T3 were obtained from Open Biosystems. The non-target pLKO.1-scrambled shRNA (designated non-target-RNAi) was from Sigma. To prepare viral particles, 293T cells were co-transfected with 750 ng of psPAX2 packaging plasmid, 250 ng of pMD2.G envelope plasmid, and 2 μg of viral vector using Fugene6. Supernatants containing lentivirus particles were collected 36–60 h of post-transfection and filtered.

For lentivirus infection, PLC/PRF/5 or NIH3T3 cells in Dulbecco's modified Eagle's medium with 10% fetal bovine serum or BS and 8 μg/ml polybrene were incubated with an equal volume of lentivirus for 24 h. Stably transfected cells were selected in puromycin (2 μg/ml for PLC/PRF/5, 3 μg/ml for NIH3T3) and tested for 14-3-3ε expression by Western blot.

Quantitative Real-time RT-PCR—Total RNA was collected with the RNeasy Mini Kit (Qiagen) and subjected to the RT reaction using oligo-dT primer and ImProm-II Reverse Transcriptase (Promega) according to the manufacturer's instruction. Quantitative real-time PCR for murine Gli1 and Ptch1 genes was performed using the cDNA of NIH3T3 cells treated with DMSO or 100 nM SAG ± 1 μM FSK. The following primers were used: Gli1: gga agt cct att cac gcc ttg a (sense) and caa cct tct tgc tca cac atg taa g (antisense); Ptch1: CTC TGG AGC AGA TTT CCA AGG (sense) and TGC CGC AGT TCT TTT GAA TG (antisense). All assays were performed with FastStart Universal SYBR Green Master (ROX) (Roche) and ABI Prism 7000 Sequence Detection Systems (Applied Biosystems). The standard curve method was used to calculate target gene expression, which was normalized to that of the *Gapdh* gene. Each sample was analyzed in duplicate.

Immunofluorescence Microscopy—Immunofluorescence microscopy was carried out as previously described (11). HeLa cells were transfected with expression vectors 24 h after seeding. After another 36 h, including 12 h exposure to 40 μM FSK in the growth medium, the cells were fixed with 2% paraformaldehyde for 15 min at room temperature, rinsed with phosphate-buffered saline (PBS), and permeabilized with 0.25% Triton X-100/PBS for 15 min. After blocking, the cells were incubated with anti-Myc Ab (1 μg/ml) overnight at 4 °C and then with Alexa Fluor 488 goat anti-mouse IgG secondary Ab (1:100 dilution) for 1 h at room temperature. The nuclei of the cells were stained with propidium iodide (Sigma). Fluorescence images were obtained using a Leica TCS SL confocal laser-scanning microscope (Leica Microsystems, Wetzler, Germany) and photographed using Leica confocal software (Leica Microsystems).

Luciferase Assays—Luciferase assays were performed as described previously (11). Approximately 1 × 10^5 293T cells were plated into each well of a 12-well tissue culture plate (Iwaki Glass, Chiba, Japan) and transiently transfected after 24 h. The transfection mixtures contained 250 ng of GliBS-Luc, 125 ng of PKA-CA, 2.5 ng of pRL-SV40 (internal control), and 125 ng of effector construct or empty vector. The cells were harvested 24 h after transfection and assayed for luciferase activity using the PicaGene Dual SeaPansy System (Toyo Ink, Tokyo, Japan) and a luminometer (Lumat LB 9507; EG & G Berthold, Bad Wildbad, Germany). Independent experiments were performed at least three times.

Electrophoretic Mobility Shift Assays—Expression vectors for constitutively active PKA-CA and for FLAG-tagged wt and S956A Gli2 were co-transfected into 293T cells in 10-cm tissue culture dishes. The cells were lysed in 1 ml of lysis buffer, and cellular proteins were immunoprecipitated with anti-FLAG Ab-conjugated agarose beads for 2 h at 4 °C. After the beads were washed with lysis buffer, the bound proteins were eluted with buffer containing 100 μg/ml of 3× FLAG peptide (Sigma).

This eluted protein lysate was used in electrophoretic mobility-shift assays performed using a LightShift EMSA Kit (Pierce Biotechnology), according to the manufacturer's instructions. Briefly, eluted protein lysate was incubated for 30 min with biotinylated DNA probe (Gli-RE) (18) and non-biotinylated competitor DNA oligonucleotide (100-fold molar excess) in binding buffer supplemented with 2.5% glycerol, 5 mM $MgCl_2$, 0.05% Nonidet P-40, and 50 ng/μl poly(dI-dC). The resulting complexes were resolved in a nondenaturing 6% polyacrylamide gel, transferred onto a membrane, and detected using HRP-conjugated streptavidin and a chemiluminescent substrate.

RESULTS

Identification of 14-3-3ε as a Novel Interacting Protein with Gli1—The MEF (Myc-TEV-FLAG) technique uses two different affinity modules (Myc and FLAG) separated by a cleavage site for the TEV protease to reduce nonspecific protein binding to the complex (Fig. 1*A*). A mammalian expression vector encoding Gli1 with an N-terminal MEF tag was constructed and transfected into 293T cells. Tagged Gli1 was then purified from cell lysates along with its bound proteins. After the proteins were eluted with FLAG peptides, they were separated by SDS-PAGE and visualized by silver staining (Fig. 1*B*). Bands detected in the Gli1 lane but not in the control lane were considered to be proteins directly or indirectly bound to Gli1. These protein bands were excised from the gel and subjected to in-gel tryptic digestion. The resultant peptides were extracted from the gel slice and analyzed using a direct nano-flow LC-MS/MS system. The corresponding proteins were identified as 14-3-3ε, semenogelin I, and 70-kDa heat-shock proteins. To confirm the interaction between Gli1 and 14-3-3ε in a physiological condition, the lysates from PLC/PRF/5 cells, where Hh signaling is constitutively active (19), were applied to immunoprecipitation using anti-Gli1 and anti-14-3-3ε Abs. As a result, Gli1 and 14-3-3ε co-precipitated each other (Fig. 1, *C* and *D*), which suggests the *in vivo* interaction of endogenous Gli1 and 14-3-3ε.

Gli1 Interacts with 14-3-3 through Ser-640—14-3-3ε is a member of evolutionarily conserved regulatory proteins that can bind to many molecules, including transcription factors (20, 21). Intriguingly 14-3-3ε is known to contribute to the neu-

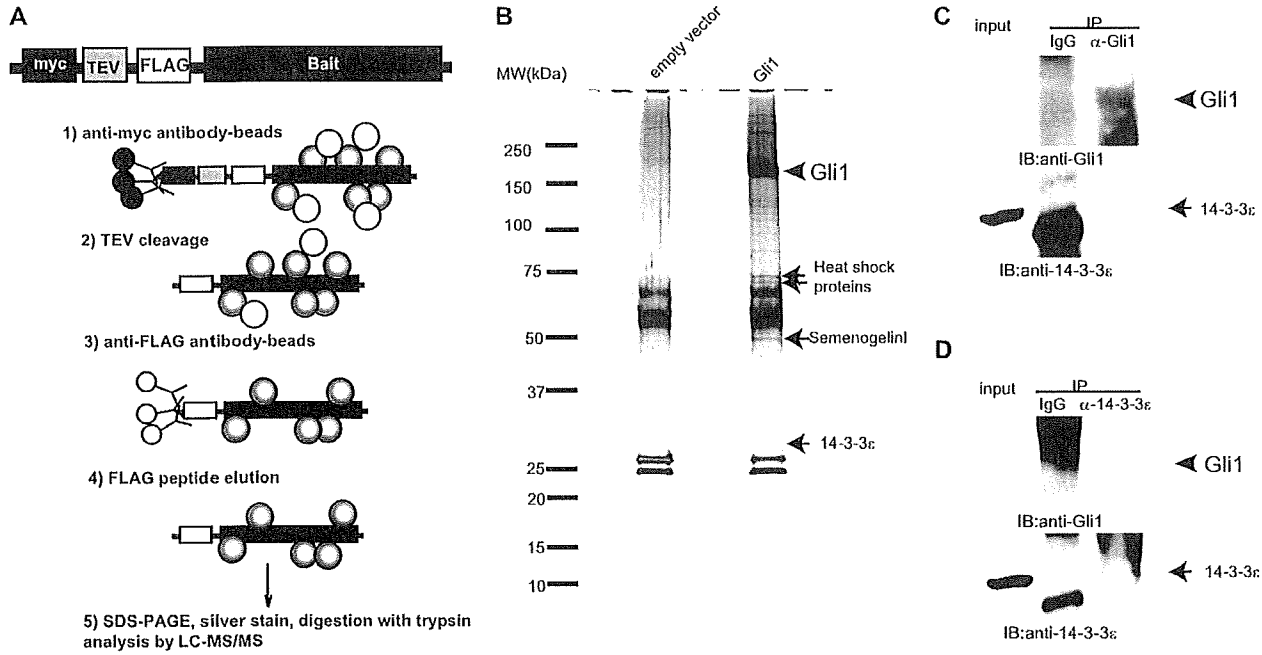

FIGURE 1. **Identification of 14-3-3ε as a Gli1-interacting protein.** *A*, schematic representation of the strategy for TAP using an MEF tag (10, 11). The pcDNA3 vector is designed to express a protein with tandem Myc and FLAG tags at the N terminus of the bait protein. The first round of affinity purification is performed using anti-Myc Ab, followed by cleavage with TEV protease. The second round of affinity purification is performed using anti-FLAG Ab, followed by specific elution with FLAG peptide. The eluted complex was separated by SDS-PAGE and silver-stained. Specific bands were digested with trypsin and analyzed by LC-MS/MS. *B*, after lysis of pcDNA3-MEF-Gli1- or pcDNA3-MEF-transfected 293T cells, the expressed Gli1 was recovered using the MEF TAP procedure. The proteins bound to Gli1 were eluted from the beads, separated by SDS-PAGE (10/20%), and silver-stained. The molecular masses of the protein are indicated. The *arrowhead* indicates the position of Gli1. The four protein bands, indicated by *arrows*, were excised from the gel and subjected to in-gel tryptic digestion. LC-MS/MS analysis identified the proteins as 14-3-3ε, semenogelin I, and 70-kDa heat-shock proteins 5, 6, and 8. *C*, lysates from PLC/PRF/5 cells were subjected to immunoprecipitation using anti-Gli1 Ab or control IgG followed by Western blotting using anti-Gli1 (*upper blot*) and anti-14-3-3ε (*lower blot*) Abs to detect endogenous interaction. *D*, immunoprecipitation using anti-14-3-3ε Ab was performed as described in *C*.

ronal development and axial patterning where Hh signaling plays important roles (22–24). 14-3-3 proteins bind to phosphoserine/threonine (pSer/pThr)-containing motifs on most of their ligands through Lys-49, a critical residue in the phospho-substrate-binding pocket (25, 17, 26). To investigate whether the interaction between Gli1 and 14-3-3 proteins is pSer/pThr-dependent, we examined the affinity of Gli1 for a K49E mutant form of 14-3-3, in which Lys-49 was replaced by Glu. We co-expressed Xpress-tagged wt or K49E 14-3-3ε with FLAG-tagged Gli1 in 293T cells and immunoprecipitated Gli1 using anti-FLAG Ab (M2) beads. As shown in Fig. 2*A*, only the wild-type 14-3-3ε, but not the K49E mutant, could be efficiently co-precipitated with Gli1. This result suggests that Gli1 interacts with 14-3-3 proteins in a phosphorylation-dependent manner.

Phospho-dependent interactions between 14-3-3 and their targets are typically mediated through the consensus 14-3-3 binding sequences, RS*X*pS*X*P or R*X*Y/FXpS*X*P, where pS is phosphoserine (or phosphothreonine) (25). To identify the site(s) on Gli1 responsible for binding to 14-3-3, we used Scansite, a Web-based peptide library-based searching algorithm that identifies sequence motifs likely to bind to specific protein domains (27). With medium stringency parameters, Scansite identified four putative serine-containing sequences (Ser-545, -640, -659, and -963) as 14-3-3-binding motifs (Fig. 2*B*). We made Ser → Ala mutations in each of these candidate sequences and performed immunoprecipitation studies using each of the mutant proteins (Gli1 S545A, S640A, S659A, and S963A). The affinity of only Gli1 S640A for 14-3-3 was significantly reduced compared with that of the wt Gli1 (Fig. 2*C*), suggesting that the phosphorylation of Ser-640 in Gli1 is critical for its interaction with 14-3-3.

14-3-3 Binding Site Is Phosphorylated by PKA in Vitro—The sequence surrounding Ser-640, RR*X*S, is identical to the consensus phosphorylation sequence for PKA. This motif is conserved in other Gli proteins, including Ci (Fig. 3*A*) and has already been reported as a putative site for PKA phosphorylation (6, 9, 28). To confirm whether PKA directly phosphorylates Gli1 Ser-640, *in vitro* kinase assays were performed. Wild-type and S640A mutant sequences flanking Gli1 Ser-640 were fused to GST and the recombinant fusion proteins examined for incorporation of ^{32}P from [^{32}P-γ]ATP by the recombinant PKA catalytic subunit. As seen in Fig. 3*B*, the wt fusion protein was efficiently phosphorylated by PKA whereas S640A mutation abolished this phosphorylation. Taken together, these data suggest that Gli1 associates with 14-3-3 proteins through Ser-640, and that PKA, a negative regulator of Hh signaling, can serve as a responsible kinase for Ser-640.

Gli2 and Gli3 Also Bind to 14-3-3 in a Phosphoserine-dependent Manner—We next examined whether Gli2 and Gli3, the other Hh-regulated transcription factors with unique roles distinct from Gli1 (1), are also phosphorylated by PKA and bind to

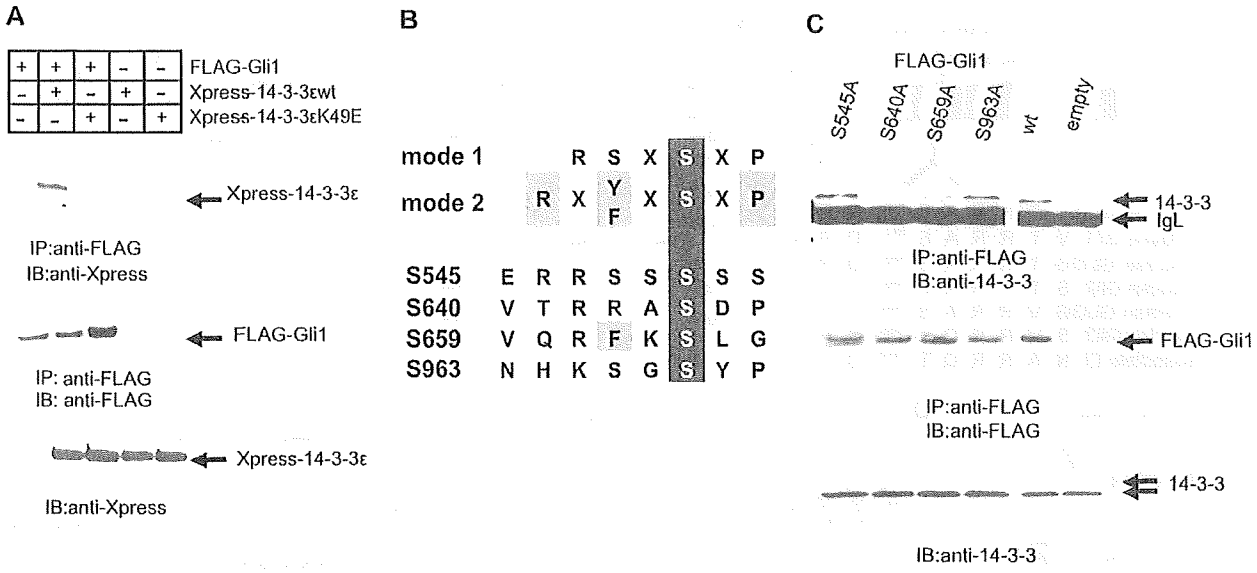

FIGURE 2. **Interaction of Gli1 with 14-3-3 through Ser-640.** *A*, Gli1 interacts with 14-3-3ε but not with the K49E 14-3-3ε mutant, which exhibited no affinity for the phosphorylated sequence. FLAG-tagged Gli1 was co-expressed with Xpress-tagged wt or K49E 14-3-3ε in 293T cells. Cell lysates were subjected to immunoprecipitation using monoclonal anti-FLAG Ab followed by Western blotting using monoclonal anti-Xpress Ab to detect associated 14-3-3ε (*upper blot*) or using anti-FLAG Ab to monitor the efficiency of Gli1 protein expression (*middle blot*). Lysate samples were also subjected to immunoblot analysis with anti-Xpress Ab (*lower blot*). *B*, Scansite prediction of the 14-3-3 binding site on Gli1. Mode1 and mode2 are consensus sequences for the 14-3-3 binding site. The amino acid sequences containing Ser-545, -640, -659, and -963 were predicted to bind to 14-3-3. *C*, Ser-640 of Gli1 is important for the interaction with endogenous 14-3-3. FLAG-tagged Gli1 proteins engineered with a Ser → Ala mutation were expressed in 293T cells. Immunoprecipitation of the cell lysates was performed with anti-FLAG Ab, followed by Western blotting using polyclonal anti-14-3-3 Ab (*upper blot*) or anti-FLAG Ab (*middle blot*). Lysate samples were also blotted using anti-14-3-3 Ab as a control (*lower blot*).

14-3-3 proteins. The amino acid sequence surrounding Ser-640 of Gli1 is highly conserved among Gli transcription factors; the corresponding serine residues in mouse Gli2 and human Gli3 are Ser-956 and -1006, respectively (Fig. 3*A*). We expressed the Gli2 and Gli3 peptides flanking these serine residues as GST fusion proteins and performed *in vitro* kinase assays with recombinant PKA. Both of the Gli2 and Gli3 fusion proteins were efficiently phosphorylated by PKA, whereas the Gli2 S956A and Gli3 S1006A mutant fusion proteins were not (Fig. 3*B*).

Next, to examine the interaction of Gli2 and Gli3 with 14-3-3, we expressed FLAG-tagged Gli2 and Gli3 in 293T cells under PKA-activated conditions, either by co-expressing the constitutively active PKA-CA (15) or by the treatment with FSK, a PKA activator. Gli2 and Gli3 were then immunoprecipitated using anti-FLAG Ab beads, and blotted for co-associated endogenous 14-3-3. As shown in Fig. 3, *C* and *D*, both the wt Gli2 and Gli3 showed strong binding to 14-3-3, whereas the Gli2 S956A and Gli3 S1006A, corresponding to Gli1 S640A, had no detectable affinity for 14-3-3, as well as the Gli3 double mutant S1006A/S1026A (Fig. 3, *C* and *D*). As an additional negative control, we also constructed Gli2 S975A and Gli3 S1026A mutants, which are analogous to the Gli1 S659A mutant. Both of these negative control mutants showed equivalent binding to 14-3-3 as the wt Gli2 and 3 proteins (Fig. 3, *C* and *D*), confirming the importance of the Gli1 Ser-640 homologs Ser-956 and Ser-1006 in Gli2 and Gli3, respectively for conferring phosphorylation-dependent 14-3-3 binding. Finally, we demonstrated that PKA induces the *in vivo* phosphorylation of the 14-3-3 consensus phospho-binding sequence R*XX*pS*X*P in Gli2, using the phosphorylation-specific Ab against this motif. In addition, we showed that the interaction of Gli2 and 14-3-3 increased in proportion to the level of Gli2 phosphorylation (Fig. 3*E*).

Binding of Gli Proteins to 14-3-3 Decreases the Hh Signaling Activity—The effect of 14-3-3 binding on the transcriptional activity of each Gli protein was examined by luciferase assay using a Gli-regulated luciferase reporter under the control of eight tandem copies of the HNF3-β Gli-binding site (8×GBS-luciferase) (13). Gli expression vectors and the 8×GBS luciferase reporter plasmid were co-transfected into 293T cells together with PKA-CA to potentiate the interaction between Gli and 14-3-3. As shown in Fig. 4*A*, co-transfection of wt Gli1 with 8×GBS-luciferase resulted in a 30-fold increase in reporter activity compared with co-transfection of 8×GBS-luciferase with vector control. The Gli1 S640A mutation up-regulated the reporter activity to the comparable level to that wt Gli1 did. Gli2 also increased reporter activity nearly 3–8-fold, and importantly, the analogous 14-3-3-binding mutant Gli2 up-regulated the activity level to more than 2-fold than that wt Gli2 did. In a while, neither wt nor the 14-3-3 binding mutant of Gli3 activated this reporter, consistent with its proposed function *in vivo* as a transcriptional repressor (12). Because deletion of the N-terminal repressor domain from Gli3 has been reported to restore its transcriptional activity (12), we constructed an N-terminal deletion mutant of Gli3 (ΔN-Gli3). We found that ΔN-Gli3 functions as a transcriptional activator like Gli2 (Fig. 4*B*) and that ΔN-Gli3 defective in 14-3-3 binding demonstrated the higher activity compared with that of ΔN-Gli3 (Fig. 4, *A* and *B*). These findings support that the phos-

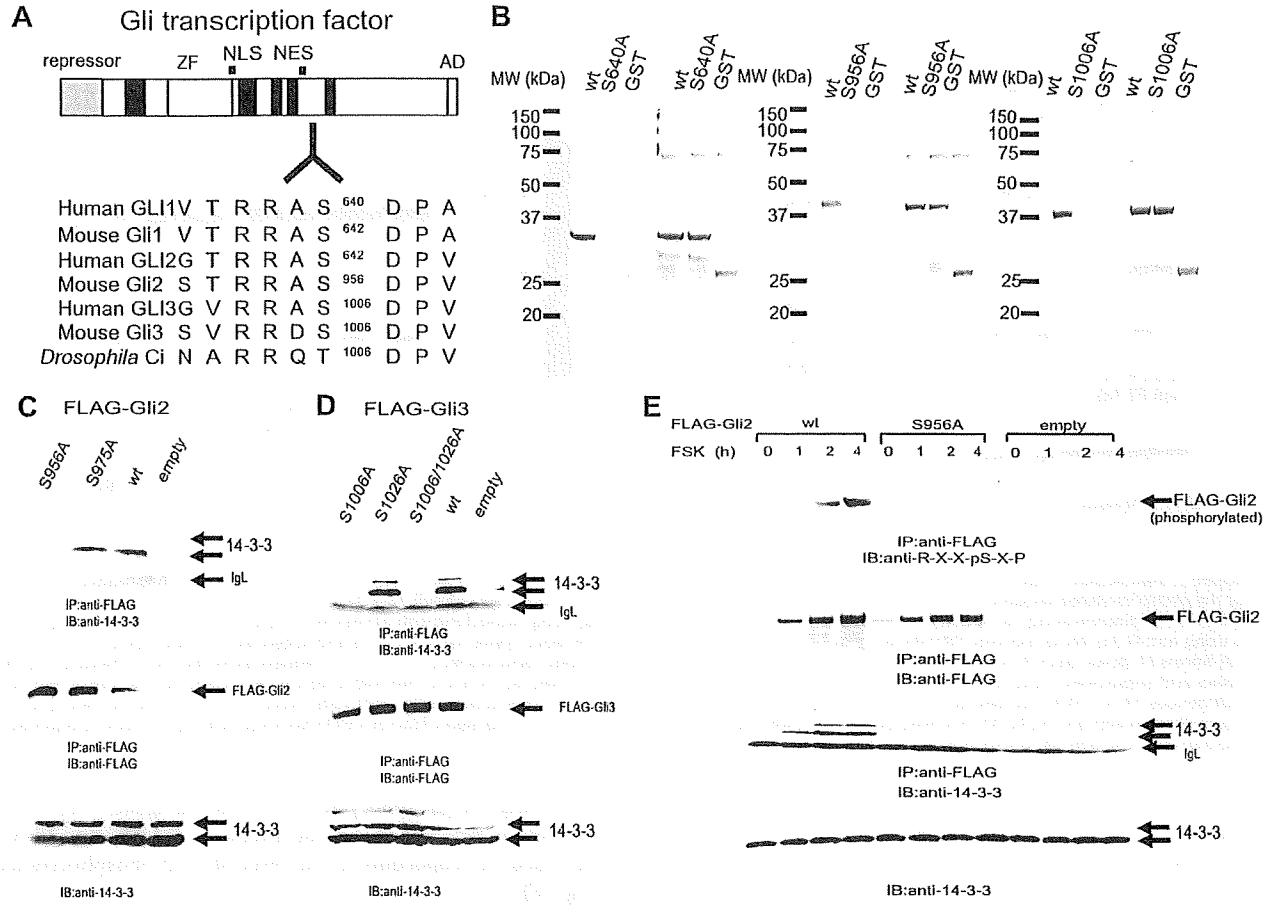

FIGURE 3. **Interaction of Gli2 and Gli3 with 14-3-3 through the conserved site phosphorylated by PKA.** *A*, schematic drawing of transcription factor Gli and conservation of its 14-3-3 binding site. *Repressor*, N-terminal repressor domain; *ZF*, zinc finger; *NLS*, nuclear localization signal; *NES*, nuclear export signal; *AD*, transactivation domain. Other conserved regions are indicated in *black*. *B*, conserved sequences of Gli1, Gli2, and Gli3 were phosphorylated by PKA *in vitro*. Kinase assays using recombinant PKA were performed with GST (about 26 kDa) or a GST fusion protein containing Gli1 Ser-640, Gli2 Ser-956, or Gli3 Ser-1006 and their respective flanking sequences (about 35, 40, or 38 kDa, respectively), in both wt and Ser → Ala-substituted forms. Reactions were resolved by SDS-PAGE, and the gel was stained with Coomassie Blue (*right panel*), dried, and analyzed by autoradiography (*left panel*). *C*, interaction of Gli2 with endogenous 14-3-3 through Ser-956. FLAG-tagged wt and mutant Gli2 (S956A or S975A) were expressed with PKA-CA in 293T cells. Cell lysates were immunoprecipitated using anti-FLAG Ab and blotted using anti-14-3-3 Ab (*upper blot*) or anti-FLAG Ab (*middle blot*). Samples of the lysates were blotted with anti-14-3-3 Ab as a control (*lower blot*). *D*, interaction of Gli3 with endogenous 14-3-3 through Ser-1006. A similar assay was performed with FLAG-tagged wt or mutant Gli3 (S1006A and/or S1026A). Wild-type and S1026A Gli3 interacted with 14-3-3, but S1006A and S1006A/S1026A mutants lost their affinity for 14-3-3. *E*, phosphorylation of Gli2 Ser-956 in 293T cells increased with FSK exposure, and the affinity of Gli2 for 14-3-3 increased as this phosphorylation increased. The 293T cells were transfected with a FLAG-tagged wt or S956A Gli2 vector or the empty vector 24 h before addition of 40 μM FSK to the growth medium. The cells were lysed after 0, 1, 2, and 4 h of FSK exposure. Lysates were subjected to immunoprecipitation using anti-FLAG Ab and blotted with Abs specific for the 14-3-3 binding site (*RXXpSXP*), FLAG, or 14-3-3. Samples of the lysates were blotted using anti-14-3-3 Ab as a control.

phorylation-dependent binding to 14-3-3 of Gli2 or Gli3 affects their transcriptional activity.

To confirm that the observed transcriptional repression requires the binding to 14-3-3 as well as the phosphorylation of Gli proteins, we constructed a new Gli2 mutant in which Pro-958 was mutated to Ala (P958A). Pro-958, which is at the +2 position relative to the pSer-956, is an important residue for 14-3-3 binding (25) but is not involved in PKA phosphorylation. As seen in Fig. 4*C*, the P958A mutation abolished 14-3-3 binding to Gli2. In luciferase assays performed under PKA-CA expression, the transcriptional activities of P958A and S956A mutants of Gli2 were comparable to each other, but 2~3-fold higher compared with those of wt or S975A Gli2 (Fig. 4*D*). These results suggest that 14-3-3 binding is essential for the phosphorylation-dependent repression of Gli transcriptional activities.

A recent report suggested that the phosphorylation of Gli2 by PKA, CKI, or GSK-3β, influences the transcriptional activity through its ubiquitination and degradation (28). In addition, phosphorylation-dependent 14-3-3 binding of MDMX has been reported to influence its ubiquitination and degradation (29). To address whether the proteasome-dependent degradation affects the 14-3-3-dependent repressive effect, we generated the Gli2 mutant lacking the regions essential for its degradation by the E3 ubiquitin ligase β-TrCP (ΔPKA). The deleted region containing the four responsible PKA phosphorylation sites, Ser-789, -805, -817, and -848 for degradation does not include Ser-956. As shown in Fig. 4*E*, the additional mutation in

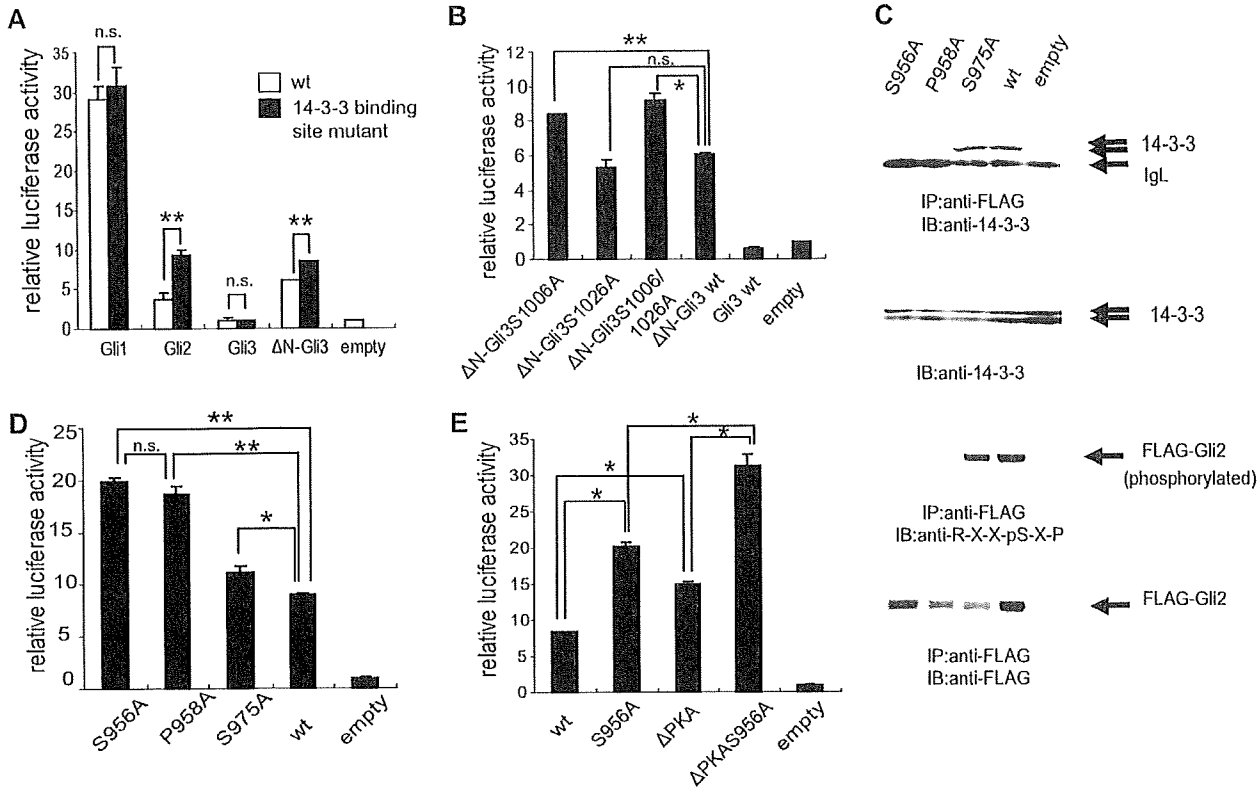

FIGURE 4. **PKA-induced interaction with 14-3-3 attenuates the transcriptional activity of Gli2 and ΔN-Gli3, a Gli3 construct lacking its N-terminal repressor domain.** *A*, 293T cells were co-transfected with Gli-BS-Luc, pRL-SV40 (internal control), PKA-CA, and a Gli1, Gli2, Gli3, or ΔN-Gli3 expression plasmid, and the luciferase activity of the wt and 14-3-3 binding site mutant Gli proteins were compared. *White bar*, wt; *black bar*, mutant. Wild-type Gli2 and ΔN-Gli3 were less active than their respective Ser → Ala mutants. *B*, transcriptional activity of Gli3 was almost equal to that of the empty vector, and deletion of the N-terminal repressor domain to create ΔN-Gli3 restored the transcriptional activity. The recovered activity of the constructs with the capacity to interact with 14-3-3 (wt and S1026A) was increased by the S1006A 14-3-3 binding site mutation (mutant S1006A and double-mutant S1006A/S1026A). *C*, Gli2 P958A mutant also lost the capacity to interact with 14-3-3, as shown by immunoprecipitation with anti-FLAG Ab and immunoblotting. Phosphorylation status could not be confirmed; however, since the proline residue at +2 relative to the putative pSer is required for detection by the anti-14-3-3 binding site Ab. *D*, transcriptional activity of Gli2 constructs was measured as described in *A* and *B*. The activities of the P958A and S956A Gli2 mutants were similar. *E*, in mutant ΔPKA-Gli2, the four regions of Gli2 containing PKA consensus sites responsible for its degradation following ubiquitination were deleted. The effect of interaction with 14-3-3 on transcriptional activity was not affected by these mutations. The data shown are representative of three independent experiments performed in duplicate (error bars). **, $p < 0.01$; *, $p < 0.05$.

Ser-956 clearly enhanced the transcriptional activity of ΔPKA Gli2, similar to the case of wt Gli2. These findings indicate that the 14-3-3-dependent repressive mechanism against Gli2 activity is independent on the degradation by the ubiquitin-proteasome system.

14-3-3 Interaction Does Not Affect the Intracellular Localization and the Relationship with SUFU of Gli2—14-3-3 binding affects the function of various proteins by sequestering from nucleus to cytoplasm (17, 20, 21). The change in the subcellular localization of Gli transcription factors, principally Ci, by their processing following PKA phosphorylation has also been investigated (7). To investigate whether 14-3-3 binding influenced the subcellular localization of Gli2, Myc-tagged wt and S956A Gli2 were expressed in HeLa cells in the presence of 40 μM FSK. Immunocytochemistry using anti-Myc antibody revealed that both wt and S956A Gli2 localized in the nucleus (Fig. 5*A*). In addition, PKA-CA and GFP-tagged Gli2 were co-expressed in 293T cells showed similar results (data not shown). Because it is reported that Gli proteins are sequestered to the cytoplasm by SUFU (14), we also examined whether 14-3-3 binding affects the interaction with SUFU. SUFU repressed the transcriptional activity of Gli2 independently of its interaction with 14-3-3 (Fig. 5*B*). The co-expression of Myc-tagged SUFU, Gli2, and PKA-CA showed that the interaction between Gli2 and 14-3-3 had no effect on the affinity of Gli2 for SUFU (Fig. 5*C*). Thus, 14-3-3 binding to Gli2 does neither affect cellular localization nor interaction with SUFU.

S956A Gli2 Protein Maintains the Affinity for Target Oligonucleotide in Vitro—To assess the direct effect of 14-3-3 on DNA binding by Gli2, we performed EMSA using immunopurified FLAG-tagged wt or S956A Gli2 from cell lysates co-expressing PKA-CA. Both wt and S956A Gli2 specifically decreased the electrophoretic mobility of the Gli-RE oligonucleotide (Fig. 5*D*). Addition of excess unlabeled Gli-RE dramatically reduced the intensity of retarded oligonucleotide bands in both the wt and S956A samples. These findings suggest that, at least in an *in vitro* condition, 14-3-3 does not affect the binding capacity of Gli2 to the synthetic naked oligonucleotides.

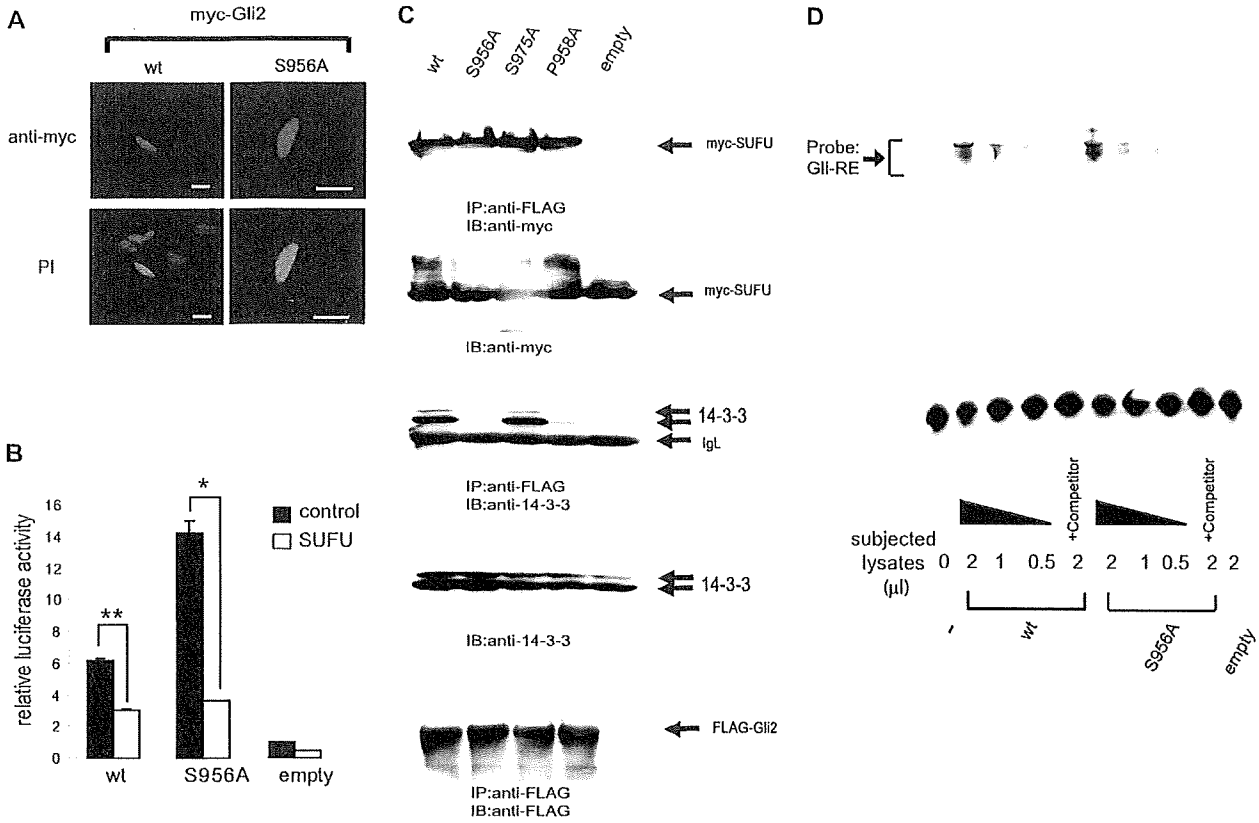

FIGURE 5. **Interaction of Gli2 with 14-3-3 does neither affect its subcellular localization, SUFU-binding activity, nor the affinity for target oligonucleotide.** *A*, neither PKA-mediated phosphorylation nor 14-3-3 binding relocalize Gli2 into the cytosol. Immunofluorescence pictures of representative HeLa cells show that both wt and S956A Gli2 localize in the nucleus in FSK-treated cells. The Myc-tagged Gli2 proteins are immunostained (*green*); the nuclei are stained with propidium iodide (*red*). *Scale bar*, 20 μm. *B*, co-expression of SUFU, which represses the transcriptional activity of both wt and S956A Gli2 and eliminates the effect of interaction with 14-3-3. The data shown are representative of three independent experiments performed in duplicate (error bars). **, $p < 0.01$; *, $p < 0.05$. *C*, immunoprecipitation using a lysate from cells co-expressing Myc-tagged SUFU, a FLAG-tagged Gli2 construct, and PKA-CA proves that 14-3-3 binding does not influence the interaction of Gli2 with SUFU. *D*, binding of Gli2 to target oligonucleotide. Cells were transiently co-transfected with expression plasmids encoding PKA-CA and FLAG-tagged wt or S956A Gli2 or the empty vector. Cell lysates were immunoprecipitated using anti-FLAG Ab, and bound proteins were eluted using 3× FLAG peptide. Eluted lysates were subjected to electrophoretic mobility shift assay. Both wt and S956A mutant Gli2 formed specific complexes with the consensus (labeled) Gli-binding oligonucleotide (*arrow*). Addition of a 100-fold excess of unlabeled Gli outcompeted the labeled oligonucleotide.

PKA Stimulation Down-regulates the Expression of Gli1, Which Is a Representative Target of Hh Signaling in a 14-3-3ε-dependent Manner—PKA is reported as a suppressor of Hh signaling by promoting degradation of Gli proteins. Given that PKA phosphorylates Gli proteins in the sites significant for 14-3-3 binding, PKA should be one of the putative kinases responsible for the 14-3-3 dependent regulation of the transcriptional activities of Gli proteins. Then we addressed whether PKA affects the transcriptional activities of Hh signaling in a 14-3-3-dependent manner. As Gli1 is a representative target protein of Hh signaling (30), the Gli1 protein level was compared between FSK-treated PLC/PRF/5 cells and DMSO-treated cells. Overnight treatment of 40 μM FSK reduced the Gli1 expression, which was consistent with the notion that PKA is a negative regulator of this signaling (6). However, in 14-3-3ε knockdown PLC/PRF/5 cells, FSK treatment reduced Gli1 protein level to a lesser extent, which suggested that 14-3-3ε played a role in PKA-dependent repression of Hh signaling (Fig. 6*A*).

To certify the effect of PKA-14-3-3 axis on Hh signaling, we also used mouse fibroblast NIH3T3, where Hh signaling is inactive. To activate Hh signaling in the cells, they were treated with SAG, which is a potent activator of Hh signaling (31). Quantitative real-time PCR showed that incubation with 100 nM SAG for 30 h induced NIH3T3 cells to express Gli1 and Ptch1 in mRNA level, and the addition of 1 μM FSK suppressed it (Fig. 6*B*). Given that Gli1 and Ptch1 are representative targets of Hh signaling, it means that SAG is able to activate Gli transcriptional activities in NIH3T3 cells. We also found that Gli1 protein as well as its mRNA was induced by the treatment of SAG (Fig. 6*C*). To elucidate the role of 14-3-3ε in the regulation of Hh signaling, we established 14-3-3ε knockdown NIH3T3 cells using lentivirus vector-based shRNA system. As shown in Fig. 6*D*, 14-3-3ε knockdown clearly canceled FSK-induced decrease in the expression of Gli1.

In addition, luciferase assay was performed using a Gli-regulated luciferase reporter, 8×GBS-luciferase. In this assay, FSK also suppressed SAG-activated luciferase activity. Furthermore, to address the contribution of 14-3-3 in this assay condition, we prepared an expression vector for the fusion protein EYFP-difopein, a specific peptide that can compete away 14-3-3

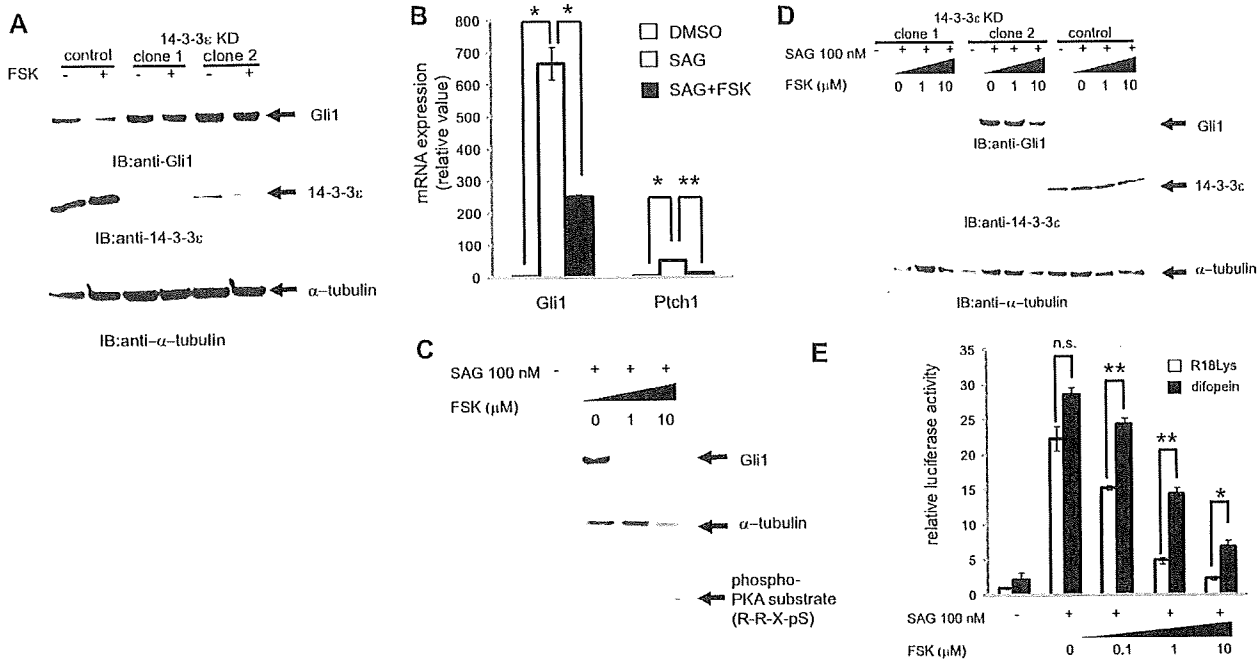

FIGURE 6. **FSK suppresses the expression of Gli1 and depletion of 14-3-3ε cancels the suppression in PLC/PRF/5 and NIH3T3.** *A*, cell lysates from PLC/PRF/5 cells, treated overnight with DMSO or 40 μM FSK, were subjected to immunoblot analysis. FSK treatment reduced Gli1 expression in control cells, but this effect was canceled in 14-3-3ε knockdown cells. 14-3-3ε knockdown was corroborated using anti-14-3-3ε and anti-α-tubulin Abs (α-tubulin: loading control). *B*, normalized Gli1 and Ptch1 mRNA levels in SAG ± FSK-induced NIH3T3 cells were determined by quantitative PCR. Cells were treated for 30 h with DMSO or 100 nM SAG ± 1 μM FSK in medium with 0.5% BS. *C*, Gli1 protein level was determined by immunoblotting. Cell lysates from NIH3T3 cells, treated as *A*, were subjected. Immunoblot using anti-phospho PKA substrate Ab showed efficient PKA phosphorylation induced by FSK (α-tubulin: loading control). *D*, cell lysates from 14-3-3ε knockdown NIH3T3 cells, treated with SAG ± FSK, were subjected to immunoblotting to determine Gli1 protein levels. 14-3-3ε knockdown was corroborated using anti-14-3-3ε and anti-α-tubulin Abs (α-tubulin: loading control). *E*, NIH3T3 cells were co-transfected with Gli-BS-Luc, pRL-SV40 (internal control), and 14-3-3 inhibitor EYFP-difopein or its control EYFP-R18Lys expression vector. After treatment as *A*, luciferase activity were determined. The data shown are representative of three independent experiments performed in duplicate (error bars). **, $p < 0.01$; *, $p < 0.05$.

from its target proteins (16). The plasmid expressing a mutated version of difopein (R18Lys) that does not inhibit 14-3-3 was used as a negative control. Interestingly, the suppressive effects of FSK treatment for Gli transcriptional activities were recognized under the co-transfection of the EYFP-difopein plasmids as well as that of EYFP-R18Lys. The level of transcriptional activities was, however, more highly induced by the co-transfection of difopein than that of R18Lys (Fig. 6*E*). These findings indicate that the molecular systems for PKA-induced suppression of Gli transcriptional activities include both 14-3-3-dependent and -independent mechanisms.

DISCUSSION

We used a proteomic approach to identify 14-3-3ε as a novel Gli-interacting protein and found that this interaction negatively regulates Hh signaling through Gli2, and an N-terminally truncated form of Gli3. This interaction depends on Gli phosphorylation, and PKA, the negative regulator of Hh signaling (32) can serve as a responsible kinase. One reported mechanism by which PKA influences Gli-dependent transcription involves the ubiquitin-dependent proteolytic processing of Gli into its repressor form (6, 9, 28); however, the PKA phosphorylated residues responsible for this processing event are different from the one for 14-3-3 binding. In addition, loss of binding to 14-3-3ε in undegradated Gli2 (ΔPKA) enhanced its transcriptional activity (Fig. 4*E*), indicating that PKA-dependent Gli binding to 14-3-3 is not involved in its ubiquitination and proteolysis. Thus, our results suggest the distinct PKA-dependent mechanisms involved in the repression of Hh signaling, through 14-3-3 binding or degradation, respectively.

Previously, 14-3-3 binding has been shown to directly affect the DNA binding activity of several transcription factors including Miz1, DAF16, and FKHRL1. Miz1 binds to 14-3-3 following AKT phosphorylation The phosphorylation/14-3-3 binding site on Miz1 is located directly in the DNA binding zinc finger region, explaining how 14-3-3 binding might reduce its affinity for DNA (33). In contrast, the DNA binding Forkhead domain in DAF-16 and FKHRL1 is distinct from the AKT phosphorylation/14-3-3 binding sites flanking both its N- and C-terminal ends (34). Similar to DAF-16 and FKHRL1, the DNA-binding regions (zinc fingers) of Gli transcription factors, are distinct from its 14-3-3 binding site (Fig. 3*A*). Thus, whereas we could not demonstrate a certain change in the binding capacity for the synthetic naked oligonucleotides by the loss of 14-3-3 binding, we do not exclude the possibility that 14-3-3 binding might reduce the affinity to target chromatin regions *in vivo*. This hypothesis might be supported by the finding that the binding of 14-3-3 to DAF-16/FKHRL induced a conformational change and altered the affinity to the *in vivo* three- dimensional DNA structures. The interaction of Gli1 and 14-3-3 was dem-

onstrated; however the overexpression of the binding mutant Gli1 did not increase the transcriptional activity (Fig. 4*A*). The binding of Gli1 to 14-3-3 might have an alternative effect for Hh signaling, different from those of Gli2 or Gli3.

The 14-3-3ϵ isoform, which we have identified here as a Gli-interacting partner, appears to play a particularly important role in neuronal development and tumorigenesis. The 14-3-3ϵ gene is located on chromosome 17p13, and heterozygous deletions in this chromosome result in human neuronal disorder, Miller-Dieker syndrome (MDS). Although mutations in the LIS1 gene *PAFAH1B1*, which is located in 17p13, contributes to MDS, the severity of MDS is suggested to be caused by the co-deletion of 14-3-3ϵ in addition to LIS1 (22). Toyo-oka *et al.* (23) showed that mice deficient in 14-3-3ϵ had defects in brain development and neuronal migration, whereas Muslin and co-workers (24) found that *Xenopus* embryos lacking 14-3-3ϵ had prominent axial patterning defects.

Inappropriate activation of Hh signaling occurs in ~60% of medulloblastomas and the most common medulloblastoma-associated genetic lesion is loss of the chromosome 17p13 region (35). This evidence supports the importance of chromosome 17p13 in neuronal development and tumorigenesis. Determining whether the novel interaction between Gli and 14-3-3, especially the 14-3-3ϵ isoform, is involved in these human neurological diseases will require further investigation.

Acknowledgments—We thank K. W. Kinzler and B. Vogelstein for human Gli1 and Gli3 cDNA; H. Sasaki for mouse Gli2 cDNA and GliBS-Luc; R. Toftgard for Myc-tagged SUFU plasmid; G. S. McKnight for the constitutively active PKA catalytic subunit expression vector; and H. Fu for EYFP-difopein and R18K expression vector. We also thank Mitsuko Tsubouchi for technical assistance.

REFERENCES

1. Hooper, J. E., and Scott, M. P. (2005) *Nat. Rev. Mol. Cell Biol.* **6,** 306–317
2. Ruppert, J. M., Kinzler, K. W., Wong, A. J., Bigner, S. H., Kao, F. T., Law, M. L., Seuanez, H. N., O'Brien, S. J., and Vogelstein, B. (1988) *Mol. Cell. Biol.* **8,** 3104–3113
3. Taipale, J., and Beachy, P. A. (2001) *Nature* **411,** 349–354
4. Ruiz i Altaba, A., Sánchez, P., and Dahmane, N. (2002) *Nat. Rev. Cancer* **2,** 361–372
5. Pasca di Magliano, M., and Hebrok, M. (2003) *Nat. Rev. Cancer* **3,** 903–911
6. Chen, Y., Gallaher, N., Goodman, R. H., and Smolik, S. M. (1998) *Proc. Natl. Acad. Sci. U.S.A.* **95,** 2349–2354
7. Chen, C. H., von Kessler, D. P., Park, W., Wang, B., Ma, Y., and Beachy, P. A. (1999) *Cell* **98,** 305–316
8. Ruppert, J. M., Vogelstein, B., Arheden, K., and Kinzler, K. W. (1990) *Mol. Cell. Biol.* **10,** 5408–5415
9. Wang, B., Fallon, J. F., and Beachy, P. A. (2000) *Cell* **100,** 423–434
10. Ichimura, T., Yamamura, H., Sasamoto, K., Tominaga, Y., Taoka, M., Kakiuchi, K., Shinkawa, T., Takahashi, N., Shimada, S., and Isobe, T. (2005) *J. Biol. Chem.* **280,** 13187–13194
11. Tanaka, Y., Kanai, F., Ichimura, T., Tateishi, K., Asaoka, Y., Guleng, B., Jazag, A., Ohta, M., Imamura, J., Ikenoue, T., Ijichi, H., Kawabe, T., Isobe, T., and Omata, M. (2006) *Oncogene* **25,** 633–642
12. Sasaki, H., Nishizaki, Y., Hui, C., Nakafuku, M., and Kondoh, H. (1999) *Development* **126,** 3915–3924
13. Sasaki, H., Hui, C., Nakafuku, M., and Kondoh, H. (1997) *Development* **124,** 1313–1322
14. Kogerman, P., Grimm, T., Kogerman, L., Krause, D., Undén, A. B., Sandstedt, B., Toftgård, R., and Zaphiropoulos, P. G. (1999) *Nat. Cell Biol.* **1,** 312–319
15. Orellana, S. A., and McKnight, G. S. (1992) *Proc. Natl. Acad. Sci. U.S.A.* **89,** 4726–4730
16. Masters, S. C., and Fu, H. (2001) *J. Biol. Chem.* **276,** 45193–45200
17. Kanai, F., Marignani, P. A., Sarbassova, D., Yagi, R., Hall, R. A., Donowitz, M., Hisaminato, A., Fujiwara, T., Ito, Y., Cantley, L. C., and Yaffe, M. B. (2000) *EMBO J.* **19,** 6778–6791
18. Pavletich, N. P., and Pabo, C. O. (1993) *Science* **261,** 1701–1707
19. Tada, M., Kanai, F., Tanaka, Y., Tateishi, K., Ohta, M., Asaoka, Y., Seto, M., Muroyama, R., Fukai, K., Imazeki, F., Kawabe, T., Yokosuka, O., and Omata, M. (2008) *Clin Cancer Res.* **14,** 3768–3776
20. Hermeking, H. (2003) *Nat. Rev. Cancer* **3,** 931–943
21. Aitken, A. (2006) *Semin. Cancer Biol.* **16,** 162–172
22. Kato, M., and Dobyns, W. B. (2003) *Hum. Mol. Genet.* **12,** R89–R96
23. Toyo-oka, K., Shionoya, A., Gambello, M. J., Cardoso, C., Leventer, R., Ward, H. L., Ayala, R., Tsai, L. H., Dobyns, W., Ledbetter, D., Hirotsune, S., and Wynshaw-Boris, A. (2003) *Nat. Genet.* **34,** 274–285
24. Lau, J. M., Wu, C., and Muslin, A. J. (2006) *Dev. Dyn.* **235,** 1761–1776
25. Yaffe, M. B., Rittinger, K., Volinia, S., Caron, P. R., Aitken, A., Leffers, H., Gamblin, S. J., Smerdon, S. J., and Cantley, L. C. (1997) *Cell* **91,** 961–971
26. Zhang, L., Wang, H., Liu, D., Liddington, R., and Fu, H. (1997) *J. Biol. Chem.* **272,** 13717–13724
27. Yaffe, M. B., Leparc, G. G., Lai, J., Obata, T., Volinia, S., and Cantley, L. C. (2001) *Nat. Biotechnol.* **19,** 348–353
28. Pan, Y., Bai, C. B., Joyner, A. L., and Wang, B. (2006) *Mol. Cell. Biol.* **26,** 3365–3377
29. LeBron, C., Chen, L., Gilkes, D. M., and Chen, J. (2006) *EMBO J.* **25,** 1196–1206
30. Dai, P., Akimaru, H., Tanaka, Y., Maekawa, T., Nakafuku, M., and Ishii, S. (1999) *J. Biol. Chem.* **274,** 8143–8152
31. Chen, J. K., Taipale, J., Young, K. E., Maiti, T., and Beachy, P. A. (2002) *Proc. Natl. Acad. Sci. U.S.A.* **99,** 14071–14076
32. Lepage, T., Cohen, S. M., Diaz-Benjumea, F. J., and Parkhurst, S. M. (1995) *Nature* **373,** 711–715
33. Wanzel, M., Kleine-Kohlbrecher, D., Herold, S., Hock, A., Berns, K., Park, J., Hemmings, B., and Eilers, M. (2005) *Nat. Cell Biol.* **7,** 30–41
34. Cahill, C. M., Tzivion, G., Nasrin, N., Ogg, S., Dore, J., Ruvkun, G., and Alexander-Bridges, M. (2001) *J. Biol. Chem.* **276,** 13402–13410
35. Ferretti, E., De Smaele, E., Di Marcotullio, L., Screpanti, I., and Gulino, A. (2005) *Trends Mol. Med.* **11,** 537–545

Scandinavian Journal of Gastroenterology, 2009; 44: 1115–1120

informa
healthcare

ORIGINAL ARTICLE

Assessment of liver stiffness in patients after living donor liver transplantation by transient elastography

RYOTA MASUZAKI[1], NORIYO YAMASHIKI[2], YASUHIKO SUGAWARA[2], HARUHIKO YOSHIDA[1], RYOSUKE TATEISHI[1], SUMIHITO TAMURA[2], JUNICHI KANEKO[2], KIYOSHI HASEGAWA[2], NORIHIRO KOKUDO[2], MASATOSHI MAKUUCHI[2] & MASAO OMATA[1]

[1]*Department of Gastroenterology, and* [2]*Division of Artificial Organ and Transplantation, Department of Surgery, University of Tokyo*

Abstract

Objective. Recurrence of hepatitis and progression of fibrosis are major problems in liver transplantation (LT) for patients with hepatitis C. Liver stiffness measurement (LSM) by transient elastography correlates well with histologic liver fibrosis stages in chronic liver diseases. The aim of this study was to evaluate the usefulness of transient elastography for the assessment of fibrosis in patients after living donor LT. ***Material and methods.*** Seventy-nine patients who visited our institution, and in whom LSM was successfully evaluated, were enrolled in the study. The patients were divided into three groups according to positivity for hepatitis C antibody and hepatitis B surface antigen as the hepatitis C virus (HCV) group ($n=37$), the hepatitis B virus (HBV) group ($n=10$), and the NBNC (negative for both hepatitis B and C) group ($n=32$). The correlation between LSM and histologic fibrosis stage was assessed in 36 patients. LSM was also compared with regard to the effect of interferon therapy in HCV patients. ***Results.*** The median value for liver stiffness was 6.8 kPa and the median time from LT was 3.1 years. In patients who underwent liver biopsy, stiffness was significantly correlated with the stages of fibrosis ($p<0.001$, rho $=0.848$). In patients who received interferon therapy after LT, the LSM decreased over time in those with a sustained virological response, whereas LSM increased in patients without a response. ***Conclusion.*** Transient elastography may be an appropriate non-invasive procedure to sequentially assess the progression of liver fibrosis in patients after LT.

Key Words: *Living donor liver transplantation, liver fibrosis, transient elastography*

Introduction

Chronic hepatitis C virus (HCV) infection leading to liver cirrhosis and hepatocellular carcinoma (HCC) is the main indication for liver transplantation (LT) in Japan and Western countries [1,2]. HCV infection recurs universally and persists after LT and has become the most relevant problem of transplant programs [3]. HCV-induced graft hepatitis and fibrosis occur in 75–80% and 10–30% of recipients, respectively, at 5 years, [4–7]. Furthermore, cholestatic hepatitis can occur in approximately 10% of patients and leads to graft failure and death [8]. As a result of this accelerated disease course, the long-term survival of graft and patient is substantially reduced in those undergoing LT for HCV-related cirrhosis compared with other groups [9].

Although still controversial, recent findings suggest that living donor liver transplantation (LDLT) might be disadvantageous for HCV-positive patients, leading to more rapidly progressive recurrent hepatitis C after transplantation [10–13]. In 1996, the first LDLT for HCV-related cirrhosis was carried out at our institution and rapid HCV replication was observed in the early postoperative days. From this experience, we adopted pre-emptive combination therapy of interferon (IFN) and ribavirin in all HCV-positive patients who underwent LDLT [14].

Correspondence: Haruhiko Yoshida, MD, Department of Gastroenterology, University of Tokyo, 7-3-1 Hongo, Bunkyo-ku, Tokyo 113-8655, Japan. Tel: +81 3 3815 5411. Fax: +81 3 3814 0021. E-mail: yoshida-2im@h.u-tokyo.ac.jp

(Received 10 May 2009; accepted 25 May 2009)

ISSN 0036-5521 print/ISSN 1502-7708 online
DOI: 10.1080/00365520903078810

Currently, the only way to assess the severity of recurrent hepatitis after LT is by means of frequent liver biopsies, which have become a part of the routine follow-up of HCV-infected liver transplant recipients. The presence of significant liver fibrosis at 1 year after transplantation identifies patients at high risk of graft loss [7,15]. One of the limitations of liver biopsy is sampling variability, which can be critical in individuals with rapid disease progression [16,17]. In addition, liver biopsy is associated with infrequent but potentially serious complications, such as bleeding. Therefore, non-invasive assessment of liver fibrosis would be a very useful tool, to reduce the number of biopsies in transplant patients.

A recently introduced technique, transient elastography, non-invasively measures hepatic elasticity, or stiffness [18–24]. A number of reports confirmed the correlation between the degree of liver fibrosis and liver stiffness measurement (LSM) in chronic liver disease [18–23]. However, neither differences in LSM among etiologies nor changes in LSM over time after LT were described.

We conducted this study to evaluate the usefulness of transient elastography as a non-invasive method of assessing fibrosis progression in patients after LT.

Material and methods

Patients

Between November 2006 and November 2008, a total of 83 patients visited the liver transplant clinic at our institution. LSM was successfully measured in 79 patients; 1 patient with ascites was excluded because fluid inhibits the measurement of stiffness by terminating the propagation of elastic shear wave, and another 3 patients with left liver grafts were excluded because a sufficient portion of liver was not observed from the right intercostal space. Details of the LDLT procedures have been described elsewhere [2,25]. The patients were divided into three groups according to the positivity for hepatitis C antibody and hepatitis B surface antigen pretransplantation as the HCV group (hepatitis C antibody positive, $n=37$), the HBV group (hepatitis B antibody positive, $n=10$), and the NBNC group (negative for both hepatitis C antibody and hepatitis B surface antigen, $n=32$). The study protocol conformed to the ethics guidelines of the 1975 Helsinki Declaration and was approved by the institutional review board (No. 1383). Patients were enrolled after written informed consent had been obtained.

Transient elastography

FibroScan (EchoSens, Paris, France) is a medical device specifically designed for hepatic transient elastography. An ultrasonic transducer is mounted on the axis of a vibrator that induces an elastic shear wave into the liver and its propagation velocity is measured by pulse-echo ultrasound acquisitions. The procedure is performed on the right lobe of the liver through an intercostal space, where intrahepatic transit is at least 6 cm thick, free of large vascular structures. Only LSMs obtained in at least eight successful acquisitions with a success rate of at least 60% were considered reliable.

Liver biopsy

Liver biopsy was performed under ultrasonography by experienced surgeons using a 16 G Bard Monopty (Medicon Inc., Osaka, Japan) needle [26] in patients who showed elevated transaminase levels and were suspected of either rejection or recurrence of hepatitis during the follow-up after LDLT. Liver biopsy specimens were fixed in formalin and paraffin embedded. All biopsy specimens were analyzed by two experienced hepatopathologists. Liver fibrosis was staged on a 0–4 scale according to the classification of Desmet and colleagues (F0, no fibrosis; F1, mild fibrosis; F2, moderate fibrosis; F3, severe fibrosis; F4, cirrhosis) [27]. Liver biopsies assessed in this study were taken within 6 months of LSM.

Postoperative care

Continuous intravenous infusion of tacrolimus was given at a dose of 2.5 $\mu g\ kg^{-1}\ h^{-1}$ just after the operation. After the whole blood level of FK reached 17–18 ng/ml, the dose was adjusted to maintain this level during the first week after the operation.

Intravenous methylprednisolone was started during the operation (20 $mg\ kg^{-1}\ day^{-1}$) and gradually tapered afterwards. When gastrointestinal function returned, treatment with FK and prednisolone was given orally (twice a day before meals). Four to 7 days after LDLT, the treatment was switched from the intravenous to the oral route.

All the hepatitis C patients pre-emptively received antiviral therapy using IFN-alfa2b or pegylated IFN-alfa2b with ribavirin, which was started as soon as possible (range, 17–46 days; median 30 days after LDLT). The therapy was started when the leukocyte level was $\geq$4000/ml, platelet count was $\geq$90,000/ml, and the hemoglobin was $\geq$10 g/dl. The therapy was discontinued when there was significant leukopenia (<1500/ml), thrombocytopenia (<50,000/ml) despite application of granulocyte colony-stimulating factor, hemolytic anemia (hemoglobin <8 g/dl), renal dysfunction (serum creatinine >2 mg/dl), depressive psychological status, or general fatigue. A sustained virological response (SVR) was defined

as undetectable HCV-RNA at least 24 weeks after the end of therapy.

Statistical analysis

Quantitative variables are expressed as medians (25th–75th percentiles). The categorical variables were compared by χ^2 tests, whereas an unpaired Student's *t*-test was used to compare continuous variables. *Post-hoc* multiple comparisons were made by analysis of variance (ANOVA) and the Tukey and Kramer test [28,29]. The correlation between LSM and histologic fibrosis stage was assessed in 36 patients who underwent liver biopsies, and the Spearman correlation was calculated between LSM and fibrosis stage. We plotted the relation between LSM and the time after LT to assess changes in LSM over time and compared LSM with regard to the effect of IFN therapy in HCV patients. A two-sided *p*-value of less than 0.05 was considered statistically significant. Statistical analysis was performed with SPSS software version 9.0 (SPSS Inc., Chicago, Ill., USA).

Results

Patients' characteristics

The pretransplant profiles of the patients are presented in Table I. Fifty-six percent were men with a median age of 54 (49–58) years. Precedent LDLT was indicated for HCV-related cirrhosis with or without HCC in 37 patients, HBV-related cirrhosis with or without HCC in 10 patients, primary biliary cirrhosis in 17 patients, autoimmune hepatitis in 2 patients, cryptogenic cirrhosis in 2 patients, fulminant hepatic failure in 10 patients, and citrullinemia in one patient. Patients' characteristics at LSM are listed in Table II. The median value of liver stiffness was 6.8 kPa. The median time from LT was 3.1 years. LSM was significantly different among the groups ($p=0.0035$ by ANOVA). The *post-hoc* test showed that the HCV group had significantly higher LSM than the other two groups.

LSM and liver biopsy

Thirty-six patients underwent liver biopsies owing to suspected rejection in 14 and suspected recurrence of hepatitis or progression of fibrosis in 22. There were no biopsy-related complications. Scatter plots of LSM for each fibrosis stage are depicted in Figure 1. LSM was significantly different between patients according to their fibrosis stage ($p<0.001$ by ANOVA) and significantly correlated with fibrosis stage. ($p<0.0001$ by Spearman's rank correlation coefficient, rho $=0.848$, $Z=5.015$). The area under the receiver operating characteristic curve (AUROC) is the most commonly used method of summarizing the overall accuracy, where an area of 1 represents a perfect test and an area of 0.5 denotes a non-informative test. The optimal LSM cut-off value was selected to maximize the sum of sensitivity and specificity based on the Youden Index [30]. AUROC for the distinction between F0–F2 and F3–F4 was 0.956 and that for the distinction between F0 and F1–4 was 0.983. The cut-off value for F0–F2 and F3–F4 was 11.7 kPa (sensitivity, 0.50; specificity, 0.94) and for F0 and F1–F4 the cut-off was 5.2 kPa (sensitivity, 0.80; specificity, 0.96).

Table I. Baseline characteristics of patients at time of LT*.

Variables	$n=79$
Age (years)	54.4 (48.9–58.1)
Gender (male:female)	44:35
Body mass index (kg/m^2)	22.3 (20.4–24.3)
UNOS status (1/2A/2B/3)	10/16/52/1
Indications	
HCV-related cirrhosis	37
HBV-related cirrhosis	10
Primary biliary cirrhosis	17
Autoimmune hepatitis	2
Cryptogenic cirrhosis	2
Fulminant hepatic failure	10
Metabolic disease	1
Graft type (L†/R‡/RLS§)	24/47/8
Laboratory data	
ASAT (IU/l)	71.0 (47.3–106.5)
ALAT (IU/l)	50.0 (28.3–72.3)
Albumin (g/dl)	2.9 (2.6-3.2)
Bilirubin (mg/dl)	3.6 (2.1–12.9)
Platelet count (10^9/l)	67.0 (43–109)
Prothrombin activity (%)	47.5 (38.6–57.2)
Creatinine (mg/dl)	0.77 (0.62–0.98)

Abbreviations: LT = liver transplantation; HCV = hepatitis C virus; HBV = hepatitis B virus; IU = international units; ASAT = aspartate aminotransferase; ALAT = alanine aminotransferase.
*Expressed as medians (25th–75th percentiles); †left liver with or without caudate lobe; ‡right liver; §right lateral sector.

LSM and time from liver transplantation

The median values for stiffness were 7.2, 4.3, and 5.5 kPa in the HCV, HBV, and NBNC groups, respectively. The HCV group is depicted in Figure 2. At the time of stiffness measurement, 9 of 37 patients with HCV infection had attained a SVR (open circles) while the other 28 patients did not (filled circles). LSM increased over time in patients without a SVR, whereas it remained low irrespective of time from LT in patients with a SVR, although the correlation coefficient was not significant. The difference in mean LSM between SVR ($n=8$) and non-SVR ($n=16$) patients was significant when LSMs taken

Table II. Baseline characteristics of patients at the time of measuring liver stiffness*.

Variables	HCV group $n=37$	HBV group $n=10$	NBNC group $n=32$	p-value (by ANOVA)
Age (years)	58.2 (55.0–62.2)	56.9 (53.9–62.0)	55.7 (45.9–62.3)	0.4737
Liver stiffness	7.2 (5.3–9.7)	4.3 (3.0–5.9)	5.5 (4.4–6.3)	0.0035
Laboratory data				
ASAT (IU/l)	23 (20–31)	16 (13–20)	19 (14–24)	0.1138
ALAT (IU/l)	20 (14–30)	17 (9–22)	14 (10–24)	0.5767
Albumin (g/dl)	3.8 (3.0–4.1)	4.4 (3.9–4.8)	3.9 (3.8–4.1)	0.1055
Bilirubin (mg/dl)	0.7 (0.6–0.9)	1.0 (0.6–1.1)	0.8 (0.6–0.9)	0.6951
Platelet count (10^9/l)	199 (156–234)	198 (167–250)	202 (168–209)	0.6924
Time from LT (years)	2.8 (1.7–4.2)	2.3 (1.6–4.4)	4.2 (2.2–5.4)	0.0533

Abbreviations: HCV = hepatitis C virus; HBV = hepatitis B virus; NBNC = negative for both hepatitis B and C; ASAT = aspartate aminotransferase; ALAT = alanine aminotransferase; IU = international units; LT = liver transplantation.
*Expressed as medians (25th–75th percentiles).

more than 2 years after transplantation were compared ($p=0.022$).

Discussion

Owing to the limitations of liver biopsies, the development of non-invasive markers of liver fibrosis has been gaining continuous interest. Several laboratory tests or combinations of tests were reported to be useful in diagnosing cirrhosis [31–34]. Benlloch et al. constructed a model to predict cirrhosis using albumin, prothrombin time, aspartate aminotransferase (ASAT), and time from LT in HCV-positive post-transplant patients and reported that the AUROC of diagnosis for cirrhosis was 0.80 in a training set of 414 patients and 0.84 in a validation set of 96 patients [35]. However, a higher AUROC for the diagnosis of cirrhosis was reported with transient elastography [36,37]. Carrion et al. evaluated the diagnostic accuracy of transient elastography to assess liver damage in 124 HCV-infected liver transplant recipients [36]. They reported that the optimal cut-off value for F2 is 8.5 kPa and that for F4 is 12.5 kPa. Moreover, with transient elastography, liver stiffness was expressed as a continuous variable. This may provide an advantage over the histologic distinction between cirrhosis and non-cirrhosis. Kazemi et al. reported that LSM was well correlated to the grade of esophageal varices ($r=0.6$, $p<0.0001$) and AUROC was 0.84 for the presence of esophageal varices [21]. Foucher et al. reported that with a negative predictable value >90%, the cut-off values for the presence of esophageal varices at stage 2 or 3, cirrhosis Child-Pugh class B or C, a past history of ascites, HCC and esophageal bleeding are 27.5, 37.5, 49.1, 53.7, and 62.7 kPa, respectively [20]. These reports suggest that transient elastography is a useful and promising

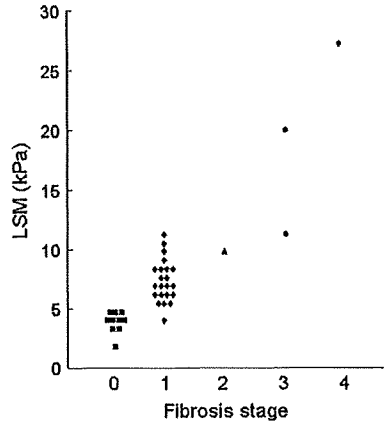

Figure 1. Liver stiffness values for each fibrosis stage.

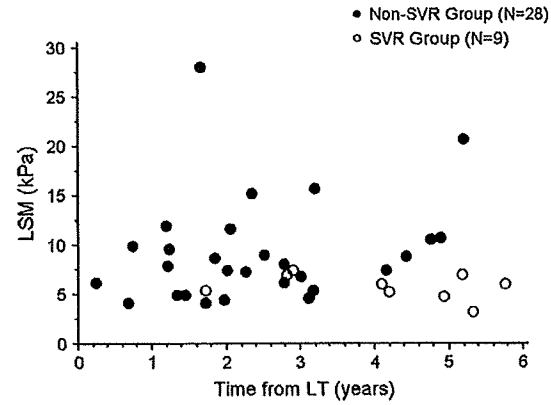

Figure 2. Hepatitis C virus (HCV) group abstracted and depicted as a scatter-plot. At the time of measurement of stiffness, out of 37 patients with HCV, 9 achieved a sustained virological response (SVR) after living donor liver transplantation (LDLT) (open circles) while another 26 did not (filled circles). Liver stiffness measurement (LSM) increased over time in patients without SVR, whereas it remained low irrespective of time from LT in patients with SVR.

test for assessing not only cirrhosis but also progression of fibrosis in a wide range of chronic liver diseases.

Recurrence of active hepatitis is the primary cause of graft loss after LT in chronic hepatitis C patients, which substantially compromises long-term survival in those patients compared with patients with other etiologies. Fibrosis progression after LT is reported to be more aggressive in hepatitis C than hepatitis B or cholestatic disease. In the current study, the LSM value was significantly higher in the hepatitis C group than in the other groups. Bahra et al. reported that the fibrosis progression rate after LT was 0.75 [38]. Once liver cirrhosis is established in an LT recipient, the probability of developing clinical decompensation within a year after diagnosis is close to 50% and, more importantly, survival after decompensation is extremely short [39].

To prevent progression of fibrosis or recrudescence of hepatitis, several tactics have been suggested. Cyclosporine has been shown to suppress an HCV replicon model as effectively as alpha-interferon *in vitro* [40], although it remains controversial whether conversion of immunosuppressive agents such as that from tacrolimus to cyclosporine has a clinically relevant antiviral effect. Combination therapy with pegylated interferon and ribavirin, currently the standard therapy for chronic hepatitis C, is also promising as an antiviral therapy for LT recipients, with reported virologic response rates of approximately 30% [41,42]. In the current study, the LSM of patients who had attained a SVR with the combination therapy after LT remained low irrespective of time from LT, whereas LSM of patients without a SVR increased over time. The increase in LSM in patients without SVR was not statistically significant, which could have been due to the small size of this study. These results indicate that fibrosis had not progressed in patients with SVR, although this is shown indirectly in the current cross-sectional study comparing the relation between LSM and time after LT.

LSM has certain limitations in practice. First, transient elastography cannot be applied to patients with ascites because elastic waves do not propagate through liquids. Second, with the current elastography device, it is required that the liver is visualized from an intercostal space with a transit of at least 6 cm. This technical requirement is sometimes difficult to meet when the liver graft is dislocated or deformed. We sometimes encountered this kind of difficulty when the left lobe graft was harvested (data not shown). Lastly, LSM could be difficult to obtain in obese patients. Foucher et al. [43] reported that a body mass index (BMI) >28 is a significant risk factor for LSM failure. In the present study, BMI ranged from 17.4 to 30.8 at the time of LSM. Only three patients exceeded 28. Specific probes are being developed for obese patients [44].

In conclusion, transient elastography may be an appropriate non-invasive procedure sequentially to assess the progression of liver fibrosis in patients after LT.

Declaration of interests: The authors report no conflicts of interest. The authors alone are responsible for the content and writing of the paper.

References

[1] European Liver Transplantation Registry. Available at: http// www.eltr.org (accessed May 2009).

[2] Sugawara Y, Tamura S, Makuuchi M. Living donor liver transplantation for hepatocellular carcinoma: Tokyo University series. Dig Dis 2007;25:310–2.

[3] Garcia-Retortillo M, Forns X, Feliu A, Moitinho E, Costa J, Navasa M, et al. Hepatitis C virus kinetics during and immediately after liver transplantation. Hepatology 2002;35: 680–7.

[4] Gane EJ, Portmann BC, Naoumov NV, Smith HM, Underhill JA, Donaldson PT, et al. Long-term outcome of hepatitis C infection after liver transplantation. N Engl J Med 1996; 334:815–20.

[5] Prieto M, Berenguer M, Rayon JM, Cordoba J, Arguello L, Carrasco D, et al. High incidence of allograft cirrhosis in hepatitis C virus genotype 1b infection following transplantation: relationship with rejection episodes. Hepatology 1999;29:250–6.

[6] Garcia-Retortillo M, Forns X, Llovet JM, Navasa M, Feliu A, Massaguer A, et al. Hepatitis C recurrence is more severe after living donor compared to cadaveric liver transplantation. Hepatology 2004;40:699–707.

[7] Berenguer M, Ferrell L, Watson J, Prieto M, Kim M, Rayon M, et al. HCV-related fibrosis progression following liver transplantation: increase in recent years. J Hepatol 2000;32: 673–84.

[8] Dickson RC, Caldwell SH, Ishitani MB, Lau JY, Driscoll CJ, Stevenson WC, et al. Clinical and histologic patterns of early graft failure due to recurrent hepatitis C in four patients after liver transplantation. Transplantation 1996;61:701–5.

[9] Forman LM, Lewis JD, Berlin JA, Feldman HI, Lucey MR. The association between hepatitis C infection and survival after orthotopic liver transplantation. Gastroenterology 2002;122:889–96.

[10] Troppmann C, Rossaro L, Perez RV, McVicar JP. Early, rapidly progressive cholestatic hepatitis C reinfection and graft loss after adult living donor liver transplantation. Am J Transplant 2003;3:239–40.

[11] Olthoff KM, Merion RM, Ghobrial RM, Abecassis MM, Fair JH, Fisher RA, et al. Outcomes of 385 adult-to-adult living donor liver transplant recipients: a report from the A2ALL Consortium. Ann Surg 2005;242:314–23, discussion 323–5.

[12] Russo MW, Galanko J, Beavers K, Fried MW, Shrestha R. Patient and graft survival in hepatitis C recipients after adult living donor liver transplantation in the United States. Liver Transpl 2004;10:340–6.

[13] Van Vlierberghe H, Troisi R, Colle I, Ricciardi S, Praet M, de Hemptinne B. Hepatitis C infection-related liver disease: patterns of recurrence and outcome in cadaveric and